SEMMELWEIS EGYETEM

DOKTORI ISKOLA

Ph.D. értekezések

3070.

BERECZKI FERENC

A támasztó és mozgató szervrendszer működésének fiziológiája

című program

Programvezető: Dr. Szőke György, egyetemi tanár

Témavezetők: Dr. Éltes Péter Endre, gerincsebész szakorvos, laborvezető és

Dr. Lazáry Áron, főigazgató helyettes, gerincsebész főorvos

IN SILICO INVESTIGATION OF THE PRIMARY STABILITY OF DIFFERENT OLIF CONSTRUCTS IN NORMAL AND OSTEOPOROTIC CONDITIONS

PhD thesis

Ferenc Bereczki

Surgical Medicine Division

Semmelweis University

Supervisors: Péter Endre Éltes, MD, Ph.D
Áron Lazáry, MD, Ph.D

Official reviewers: Fabio Galbusera, PhD
György Márk Hangody, MD, PhD

Head of the Complex Examination Committee:
Miklós Szendrői, MD, D.Sc

Members of the Complex Examination Committee:
Imre Szerb MD, PhD, Habil.
Gábor Skaliczki, MD, PhD, Habil.
Zoltán Dénes, MD, PhD

Budapest
2024

TABLE OF CONTENTS

LIST OF ABBREVIATIONS

Abbreviation	Definition
USA	United States of America
FDA	Food and Drug Administration
FE	Finite Element
FEA	Finite Element Analysis
LIF	Lumbar Interbody Fusion
OLIF	Oblique Lateral Interbody Fusion
BPS	Bilateral Pedicle Screw
LPS	Lateral Plate System
SSA	Self-anchoring Stand Alone
PMMA	Polymethylmethacrylate
TLIF	Transforaminal Lumbar Interbody Fusion
CT	Computed Tomography
PACS	Picture Archiving and Communication System
DICOM	Digital Imaging and Communications in Medicine
DSI	Dice Similarity Index
3D	3 Dimensional
STL	Stereolithography
AF	Annulus Fibrosus
NP	Nucleus Pulposus
MPa	Mega Pascal
ALL	Anterior Longitudinal Ligament
PLL	Posterior Longitudinal Ligament
LF	Ligamentum Flavum

Abbreviation	Definition
ISL	Interspinal Ligament
SSL	Supraspinal Ligament
ITL	Intertransverse Ligament
CL	Capsular Ligament
PEEK	Polyether Ether Ketone
CAD	Computer Assisted Design
AR	Aspect Ratio
FL	Follower Load
ASTM	American Society for the International Association for Testing and Materials
ROM	Range of Motion
Nm	Newton-Metre
N	Newton

1. INTRODUCTION

1.1. In Silico Medicine

The cooperation between clinicians and bioengineers has consistently demonstrated its effectiveness through the development of tools, devices, and methodologies aimed at enhancing healthcare systems. (1) Particularly within the realm of surgical intervention, the collaboration between engineers who embrace rationalism and surgeons who harness creativity has yielded unprecedented advancements and innovative solutions. (2); (3) Computational biomechanics encompasses the utilization of advanced modelling techniques for the purpose of simulating the mechanical characteristics of anatomical regions, as well as the interaction between biological structures and surgical instruments. (4); (5) The continuous enhancement in in silico modelling and computational power has led to the improvement in accuracy and reliability of computational methods. Consequently, in-silico analyses and simulations have the potential to effectively substitute, minimize, and enhance the experimentation conducted on animal, and cadaveric models. (6) This trend can already been seen as the United States of America (USA) Food and Drug Administration (FDA) has approved the use of an in silico model (diabetes type I simulator 35) to completely replace the experiments on dogs. (6)

Numerous physical phenomena within the realms of science and engineering can be described through partial differential equations characterizing variations in continuous variables. Finite element (FE) analysis serves as a computational method for addressing these differential equations. Widely employed in engineering, the FE approach facilitates solutions for stress analysis, fluid flow, electromagnetics, and heat transfer by computational models. (7) The first application of finite element analysis (FEA) in biomechanics was published by Brekelman et al. in 1972. (8) Since then, FE analysis is extensively employed in the domain of orthopaedic engineering to effectively investigate the reaction of a novel implant or device when exposed to diverse loadings. Furthermore, FE analysis possesses the capability to integrate the influence imposed by the boundaries existing between the bone and implant. (8); (9) It enables the examination and analysis of mechanical characteristics, such as structural modulus, stress distribution within intricate structures (such as a spinal vertebral body), and compressive strength. Furthermore, it serves as a proficient tool for comparative assessment of the biomechanical attributes of implants. (10); (11) Finite element analysis (FEA) has been widely employed within the

domain of spinal research, facilitating the comprehension of intricate pathologies such as scoliosis, fractures, osteoporosis, disc degeneration, and corresponding treatment modalities. (12)

1.2. The Surgical Challenges Posed by Elderly Population, and the Minimally Invasive Oblique Lateral Interbody Fusion Technique

Lumbar interbody fusion (LIF) is a gold standard surgical treatment option for a range of spinal disorders including; degenerative pathologies, infection, trauma and neoplasia. (13) LIF can be achieved via different approaches, techniques, each with their own unique instruments, implants (exp. cages) and advantages, disadvantages, indication and limitation. (14) The age structure of the global population is currently undergoing an upward shift due to decreasing fertility rates and increasing life expectancy (15) resulting in the changing epidemiology of disease and spinal disorders. (16) Advancement in minimally invasive spinal fusion technology (17) can provide an answer for the aging population challenge. (18) The minimally invasive anterior approach to the lumbar spine through retroperitoneal access was first described by Mayer in 1997. (19) Silvestre et al. (20) used Mayer's minimally invasive retroperitoneal anterior approach for lumbar interbody fusion, and it was referred to as oblique lumbar interbody fusion (OLIF). The OLIF technique, which has become a widely accepted surgical approach in the past decade, (13); (21) provides a secure access corridor from the patient's left side spanning from the L2 to the L5 vertebrae between the psoas muscle and the aorta. Through the corridor the surgeon can resect the disc, remove the cartilage endplate, insert a large intervertebral cage **(Figure 1)** and achieve the goal of intervertebral fusion and indirect decompression (22) by keeping the lumbosacral plexus safe. (21); (22); (23) During the OLIF procedure different additional fixation methods can be applied. Currently there is no consensus-based guideline about the indication for the choice of a certain type. In order to achieve stabilization, posteriorly placed percutaneous bilateral pedicle screws (BPS) can be utilized (22), which generally requires the intraoperative repositioning of the patient and additional incisions increasing the surgical time, and load as well. (24) To make the surgery less invasive, a lateral plate can be fixed with screws to the vertebral bodies through the original abdominal incision. (25) Lateral plate-screw (LPS) fixation has a longer history in spinal trauma, but new plate design has been emerged recently dedicated for OLIF. A relatively novel type of lateral plate is the Self Anchoring

Standalone (SSA) system where the plate is also attached to the intervertebral cage in addition to the vertebrae. For experienced spine surgeons there is no difference in the complexity of the 3 procedures. Biomechanical characteristics of the different OLIF constructs can significantly influence the short- and long-term implant-related complication rate as well as the possibility of achieving bony fusion thus the therapeutic outcome. Several other fixation methods and combination of these have been reported considering their technical specifications. However, only a few studies have investigated the biomechanical characteristics of OLIF with various fixation options (26); (27); (28), especially focusing on the effect of osteoporosis, which is widely present in the ageing population (16) and there can be no study found in the relevant literature aside from this thesis and the publications it is based on, where the 3 aforementioned implants are compared with osteoporotic bony conditions.

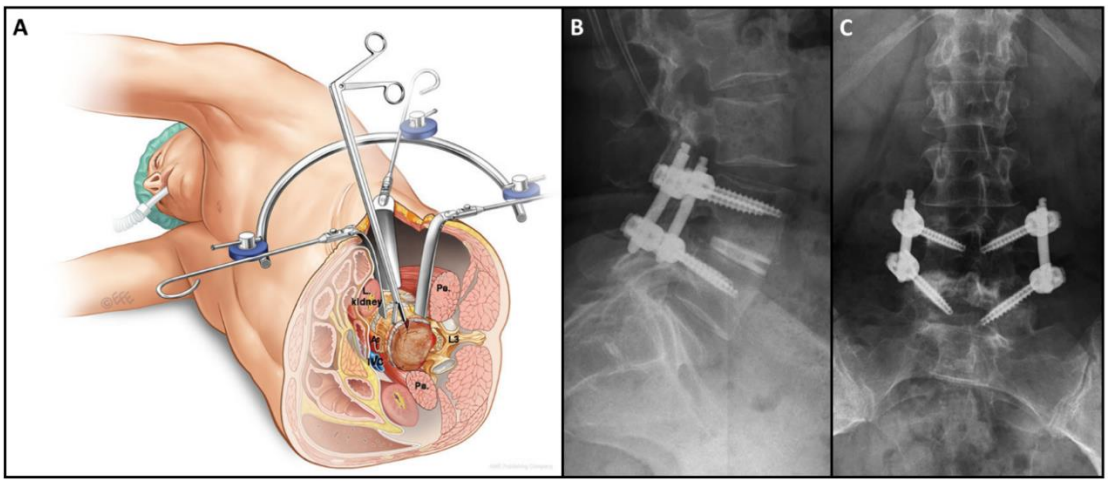

Figure 1. A: During an Oblique Lateral Interbody Fusion (OLIF) surgery, the patient is positioned in a right-side lying position. The incision is made on the left abdominal wall, and the operated motion segment is reached through the retroperitoneal area between the abdominal aorta, and the psoas muscle. (the illustration was published by Mobbs et al. (2015) and was not modified in this Figure) (13) **B:** Postoperative lateral X-ray scan of the OLIF cage, and the Bi-Pedicle Screws. **C:** Postoperative antero-posterior X-ray scan of the OLIF cage, and the Bi-Pedicle Screws.

1.3. Osteoporosis, and Polymethylmethacrylate (PMMA) Augmentation in the Field of Spine Surgery, and OLIF

Osteoporosis is a pathological condition manifested by diminished bone density, degradation of bone tissue, and disruption of bone microstructure. Specifically, individual trabecular plates of bone undergo loss, resulting in a structurally compromised framework with notably diminished mass. Individuals afflicted with osteoporosis are at an elevated risk to fractures, exacerbating due to concomitant deteriorations in physiological function associated with aging. (29) Screws placed in osteoporotic bone tend to create a clear zone around them under cyclic loading conditions, posing a higher risk of the pull-out mechanism and loosening. This phenomenon, known as osteolysis, has been thoroughly investigated by previous biomechanical studies (30); (31) In these cases, to enhance implant stability, PMMA augmentation can be used through cannulated screws. This method can successfully reduce the occurrence of implant failure and increase durability against cyclic loading. (32); (33) However, as the volume of augmented PMMA increases, so does the risk of leakage and complications. (34); (35) The aforementioned surgical technique is used in Transforaminal Lumbar Interbody Fusion (TLIF) or posterior stabilization surgeries. where the patient's bone quality can be considered poor, and the risk of screw loosening is high. (36) However, in the case of OLIF surgeries, PMMA augmentation of the laterally placed vertebral body screws is a relatively unexplored area of spine surgery and could potentially increase the primary stability of the SSA constructs, making them comparable to the BPS fixation method.

To the best of the author's knowledge, at the time of this thesis, there is currently no study in the literature analysing the possible biomechanical implications of SSA implant PMMA augmentation in OLIF surgeries compared to BPS fixation with osteoporotic bony conditions.

1.4. Stanford Biodesign, a basis for innovation

Innovation is characterized by the introduction of novel ideas, creative concepts, unique methodologies, or original devices. (37) From a northern standpoint, innovation is viewed as the implementation of superior solutions that address emerging demands, undisclosed necessities, or current market requirements. (38) It is a pivotal factor in economic progress and healthcare advancement, exerting a substantial influence on society overall. The Stanford Biodesign program is a longstanding life science initiative that specializes in training emerging leaders in the field of biomedical technology, particularly in the development of medical devices. (39) A notable feature of the Stanford Biodesign approach is its emphasis on identifying and assessing clinical needs over simply adopting novel technologies, which serves. as the foundation for groundbreaking inventions. (40) This workflow was utilized as the foundation for the development of my thesis. At our Institution (National Center for Spinal Disorders, Budapest), there was an observed increase in mechanical failures in older patients undergoing OLIF surgeries using lateral plates compared to bi-pedicle screw fixation, despite the potential benefits of reduced surgical load with lateral plates. A review of the relevant literature revealed a lack of consensus on the optimal fixation options for OLIF surgeries in older population.

As the initial step of the Stanford Biodesign process, the clinical problem/need was identified and in silico medicine was employed to further investigate the clinical questions and to generate and test concepts and potential solutions.

2. OBJECTIVES

This thesis aimed to examine the primary stabilizing impact of various constructs employed in Oblique Lateral Lumbar Interbody Fusion (OLIF) surgery under normal and osteoporotic bone conditions, to provide a better understanding of the presented clinical question. The potential impact of polymethylmethacrylate (PMMA) reinforcement on these constructs was also assessed in the presence of osteoporosis to explore potential solutions/concepts for the identified clinical need, employing the basis of the Stanford Biodesign process. Finite Element (FE) analysis served as the fundamental framework for this study. The research was divided into 2 parts.

Part I:

- To establish a foundation for finite element (FE) investigations, it was imperative to construct an intact bi-segmental spinal finite element model. In order to utilize this model, it was essential to undergo a validation process against a cadaveric in vivo specimen. To accurately simulate the impact of osteoporosis, the intact model had to be modified further.
- In order to generate surgical FE models, the incorporation of implant geometries were necessary. Simplified 3D implant models were derived through the process of digitalizing the implants used in OLIF surgery. A virtual surgery was performed on the intact FE models with the different investigated implant constructs (BPS, SSA, LPS) creating the surgical FE models.
- The primary biomechanical stability of three different implant constructs under normal and osteoporotic bony conditions were assessed with different anatomical loading conditions. Additionally, the impact of osteoporosis on these implant constructs were investigated further.

Part II

The effect of PMMA augmentation was the second part of this thesis. The main goal was to compare the posterior fixation method, with the lateral plates. SSA was chosen for this comparison, hence being the novel implant.

- The created SSA, and BPS surgical FE models needed to be altered for the investigations. Different volumes of custom made PMMA geometries were created based on the relevant literature, and integrated to the surgical osteoporotic FE models.
- The influence of PMMA augmentation on the examined implant constructs with osteoporotic bone was assessed by comparing the primary stability of the PMMA augmented FE models to that of the original surgical osteoporotic FE models. Additionally, comparisons were made between the two different implants to determine any differences in their effects.

3. METHODS

3.1 Part I: Development and Validation of an Intact L2-L4 Finite Element Model, Generation of Implant 3D Geometries, and the Creation of 3D Surgical Finite Element Models and Environment

Generation of an L2-4 Lumbar Spine Bi-segment Finite Element Model

A Computed Tomography (CT) scan (Hitachi Presto, Hitachi Medical Corporation, Tokyo, Japan) of a 24-year-old patient's lumbar spine was selected from a study of 270 patients who underwent different treatment due to low back pain in our clinic (MySPINE, Project ID: 269909, Funded under: FP7-ICT). The imaging protocol was previously defined in the MySPINE project, (41); (42) and the images were reconstructed with a voxel size of 0.6x0.6x0.6 mm^3. The L2-3 and L3-4 segments were not affected by any musculoskeletal pathology. The data were extracted from the hospital's Picture Archiving and Communication System (PACS) in Digital Imaging and Communications in Medicine (DICOM) file format. To comply with the ethical approval of the patient data protection, de-identification of the DICOM data was performed using the Clinical Trial Processor software (Radiological Society of North America, https://www.rsna.org/ctp.aspx) (43) In order to define the 3 Dimensional (3D) geometry, we performed segmentation procedure in Mimics image analysis software (Mimics Research, Mimics Innovation Suite v23.0, Materialise, Leuven, Belgium) via Hounsfield thresholding algorithm and manual segmentation tools. To evaluate the accuracy of the segmentation process, we calculated the Dice Similarity Index (DSI) (44); (45) based on two segmentation session of the same geometry. The DSI quantifies the relative volume overlap between two segmentations. DSI = $\frac{2 \times V(I1 \cap I2)}{V(I1)+V(I2)}$ V represents the volumetric measurement of the voxels contained within the binary mask, calculated by multiplying the number of voxels by their respective voxel size (expressed in mm^3). I_1 and I_2 represent the binary masks resulting from two distinct segmentation processes performed by two investigators (I_1 and I_2). The DSI values lie in the range of 0 to 1, with a value of 1 indicating a perfect match between the two masks. (44); (45)

From the segmented masks, a triangulated surface mesh was automatically generated in Stereolithography (STL) format. In 3-Matic (Mimics Research, Mimics Innovation Suite v21.0, Materialise, Leuven, Belgium) software surface smoothing (iteration: 6, smoothing

factor: 0.7, with shrinkage compensation) and uniform remeshing (target triangle edge length 0.6 mm, sharp edge preservation, sharp edge angle 60°) was applied on the 3D geometries.

In 3-Matic the vertebras were divided to posterior and anterior parts. (46) The anterior parts were divided to a cortical shell (thickness: 1 mm), vertebral bony endplates (thickness: 0.5 mm), and a cancellous core. Facet joints were modelled manually, with 0.25 mm cartilage height and minimum 0.5 mm gap between the two facets. (47) **(Figure 2A, 2C).** The intersection based non-manifold assembly was exported to Hypermesh software (Altair Engineering, Inc., Troy, Michigan, USA), and all of the surfaces were remeshed with a uniform triangulated surface mesh (target tringle edge length: 1 mm). From the resulted 3D surfaces, an adaptive tetrahedral volume mesh was generated, with the exception of the bony endplates where pyramid elements were used **(Table 1).**

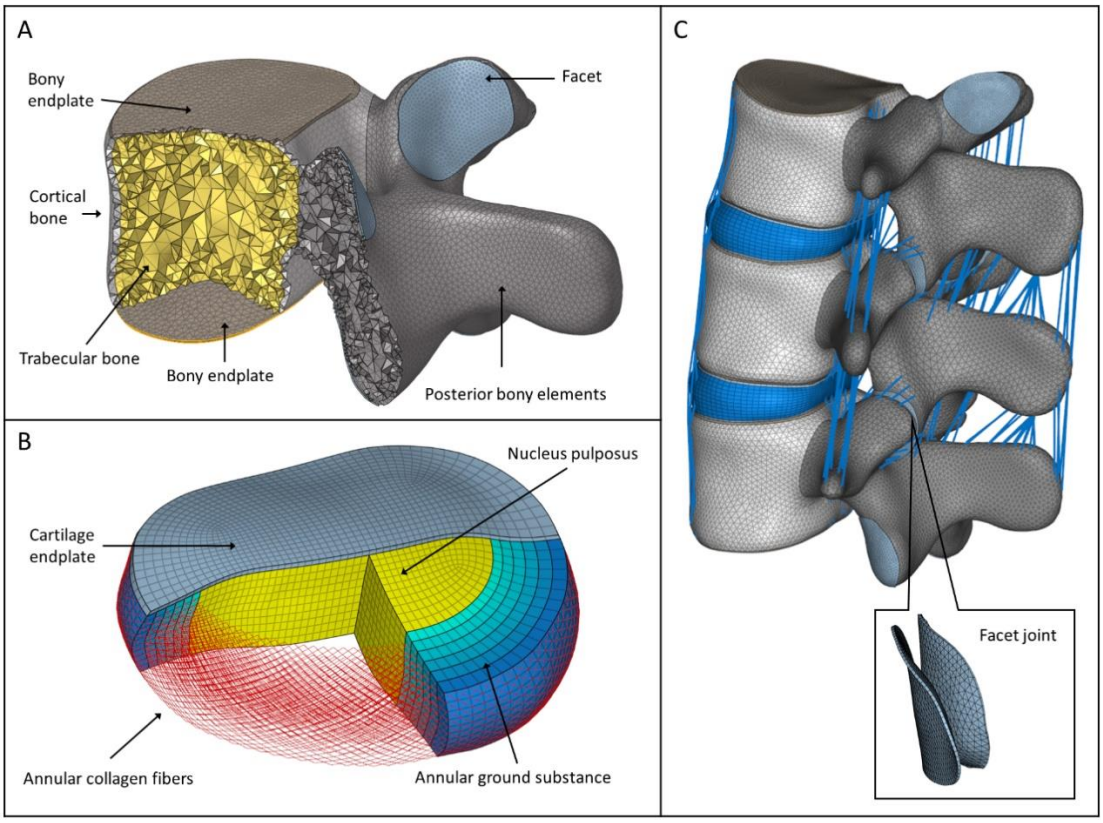

Figure 2. Finite element model of the intact L2-4 spine bi-segment. **A:** Model of the vertebral body, bony endplates, cortical shell, trabecular core, posterior elements, and articular facet. **B:** Model of the intervertebral disc, nucleus pulposus, annular collagen fibers and ground substance. **C:** Intact L2-4 lumbar spine bi-segment finite element model, with facet joints and ligaments, left postero-lateral view.

The annulus fibrosus (AF) and the nucleus pulposus (NP) defining the intervertebral disc were modelled manually according to the literature. **(Figure 2B)** (48); (49) The NP accounted for 45% of the intervertebral volume and was moved in the posterior direction, so that the sagittal thickness of the posterior AF substance became 80% of the anterior AF thickness. (48) The fluid like behaviour of the NP was modelled with an isotropic, hyperelastic Mooney-Rivlin formulation (hexahedral mesh). (49) The AF consisted of 2 times 6 annulus fiber sets embedded into a hexahedral ground substance matrix of 6 layers with alternating orientations about ±30° to the mid-cross-sectional area of the disc**.** (50) The fiber cross sectional areas were calculated by the assumed collagen fiber content fractions: 23% at the outermost layer gradually decreasing to 5% at the innermost layer. (48); (50) Cartilaginous endplate thickness was set to 0.5 mm with hexahedral elements **(Table 1).** (51)

Table 1. Applied material properties of the FE models E: Young's modulus (in MPa), ν: Poisson's ratio, *: Neo-Hooke hyperelastic model, †: Mooney-Rivlin hyperelastic model.

Material	Element type	Material Properties	References
Normal Cortical Bone	C3D4	E = 12.000; ν = 0.3	(52)
Osteoporotic Cortical Bone	C3D4	E = 8.040 (67% of normal); ν = 0.3	(53), (54), (55)
Normal Cancellous Bone	C3D4	E = 100; ν = 0.2	(52)
Osteoporotic Cancellous Bone	C3D4	E = 34 (34% of normal); ν = 0.2	(53), (54), (55)
Normal post. Elements	C3D4	E = 3.500; ν = 0.25	(56)
Osteoporotic post. Elements	C3D4	E = 2345 (67% of normal); ν = 0.25	(53), (54), (55)
Normal Bony Endplate	C3D4, C3D5	E = 1.000; ν = 0.4	(57)
Osteoporotic Bony Endpate	C3D4, C3D5	E = 670 (67% of normal); ν = 0.4	(53), (54), (55)
Cartilaginous Endplate	C3D8	E = 23.8; ν = 0.42	(50)
Facet Cartilage*	C3D6	C10=5.36; D1=0.04	(51)
Annulus Fibrosus Ground Substance*	C3D8H	C10=0.3448; D1=0.3	(58)
Annulus Fibrosus Fibre	T3D2	Cross sectional areas were calculated for each layer from volume fractions. 23% at the outermost layer to 5% at the innermost fiber layer	(56), (50)
Nucleus Pulposus†	C3D8H	C10=0.12; C01=0.03	(49)
Ligaments	SPRINGA	Nonlinear stress-strain curve	(59)
Bone Graft	C3D4	E = 100; ν = 0.2	(60)
PEEK	C3D4	E = 3.600; ν = 0.3	(61)
Titanium (screw, plate, rod)	C3D4	E = 110.000; ν = 0.3	(61)
PMMA	C3D4	E = 3.000; ν = 0.4	(62), (63)

In total, 7 ligaments were modelled as tension only spring elements with non-linear material properties. ALL (anterior longitudinal ligament), PLL (posterior longitudinal ligament), LF (ligamentum flavum), ISL (interspinal ligament), SSL (supraspinal ligament), ITL (intertransverse ligament), and CL (capsular ligament) **(Table 2).** The attachment points, orientation and the element number of the ligaments were adopted from a previous study (MySPINE, Project ID: 269909, FP7-ICT), **(Figure 2C).** The material properties were taken from the literature. (59) Facet cartilage material was described by a Neo-Hookean model, and a surface-to-surface contact without friction was set between the facet surfaces. (50)

Table 2. Properties of the ligaments (Rohlmann et al.) (59).

Ligament	Stiffness (N/mm)	Strains between (%)	Stiffness (N/mm)	Strains between (%)	Stiffness (N/mm)	Strains higher than (%)
ALL	347	0-12.2	787	12.2-20.3	1864	20.3
PLL	29.5	0-11.1	61.7	11.1-23	236	23
LF	7.7	0-5.9	9.6	5.9-49	58.2	49
CL	36	0-25	159	25-30	384	30
ITL	1.4	0-13.9	1.5	13.9-20	14.7	20
SSL	2.5	0-20	5.3	20-25	34	25
ISL	0.3	0-18.2	1,8	18.2-23.3	10.7	23.3

Cage, Implant Construct and Surgical FE Model Development

A PEEK (polyether ether ketone) OLIF cage (EMERALD™, Sanatmetal, Eger, Hungary, 45x22x12 mm, with 6º lordosis) was scanned with a ScanBox 3D scanner (Smart Optics Sensortechnik GmbH, Bochum, Germany). The obtained point-cloud was used to reconstruct the virtual 3D cage model in 3-Matic software. The model was exported in STL format to Autodesk Fusion 360 (Autodesk Inc., San Rafael, CA, USA) Computer Assisted Design (CAD) software and served as a base for creating a simplified cage mesh **(Figure 3A).** The resulted geometry was used in all three (BPS, LPS, SSA) FE models in the same central position. The L3-4 motion segment offers a relatively safe passage for the surgeon, where the ascending lumbar vein, the possible upper division of the common iliac vein, and the chest cage rarely interferes with the surgery. (64); (65) In order to simulate the surgical nucleotomy, the NP, 4 inner layers of AF and the cartilage endplates

were removed from the investigated motion-segment (L3-4), and a window was created to insert the cage from the left side of the disc **(Figure 3B).**

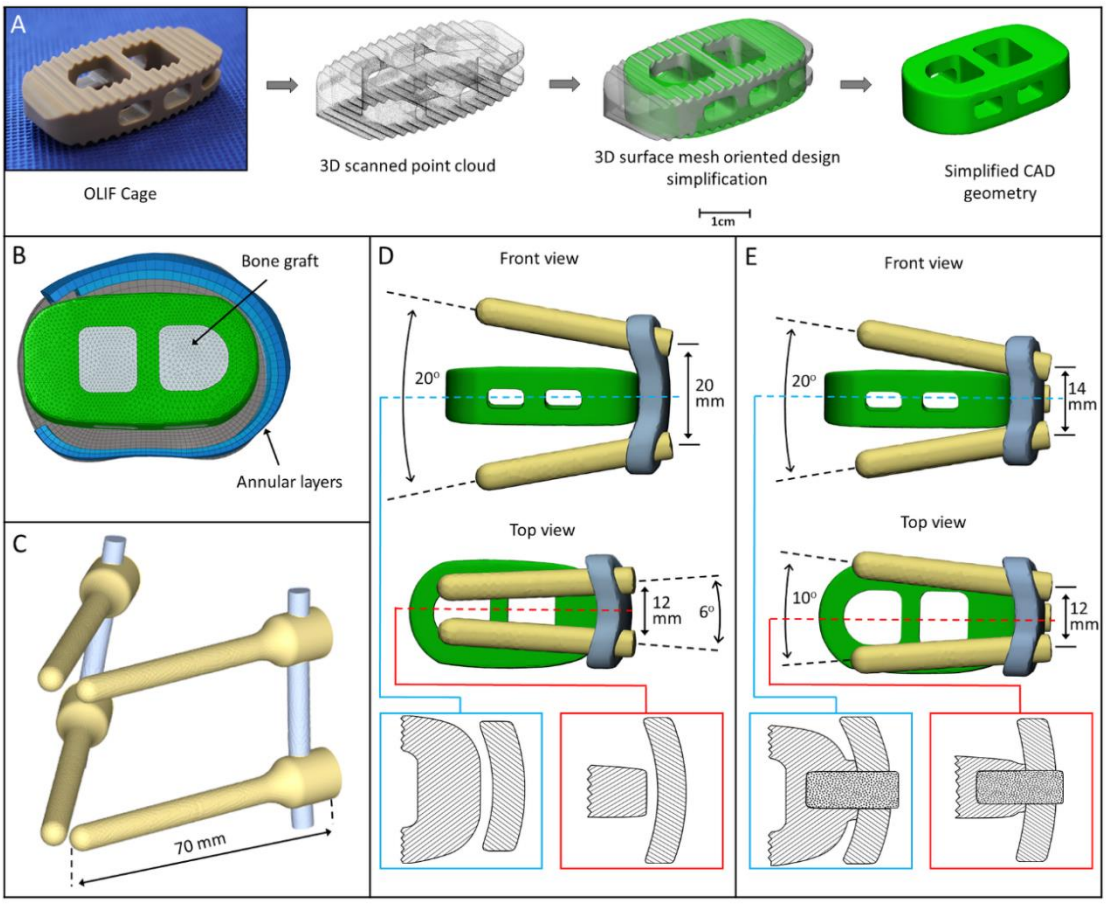

Figure 3. 3D models of the implants. **A:** Physical OLIF cage and virtually simplified CAD geometry obtained via 3D scanning (point cloud). The 3D surface mesh model oriented the design simplification process. **B:** the position of the cage inside the intervertebral space. The internal space of the cage is filled with bone graft. **C:** bilateral pedicle screw fixation model (BPS). **D:** cage model and lateral plate fixation system with screws (LPS). The cage is not connected to the plate (blue box: axial plane section, red box: sagittal plane section). **E:** the cage connects to the plate with a screw (SSA) forming a self-anchoring mechanism (blue box: axial plane section, red box: sagittal plane section).

For the BPS model 4 identical simplified transpedicular screws (70 x 5.5 mm) were placed inside the L3 and L4 pedicles. The screwheads were connected by a 5.5 mm titanium rod **(Figure 3C).** A lateral plate (32 x 23 x 4 mm) was designed to match the geometry of the L3 and L4 vertebra with a coronal and an axial curvature for the LPS model, and 4 simplified lateral screws (40 x 5.5 mm) were inserted to fix the plate. There was no connection between the plate and the inserted cage in the LPS construct **(Figure 3D).** For the SSA model a smaller bi-curved plate (26 x 23 x 4 mm) was anchored to the cage with a simplified screw (15 x 5.5 mm) and the 4 lateral screws (40 x 5.5 mm) were inserted at a different (diverging) axial angle compared to the LPS model **(Figure 3E),** "tie constrain" was defined between bone-titanium, titanium-titanium, PEEK-titanium contact surfaces, to simulate rigid fixation. To model the knurled surface of the PEEK cage, a 0.2 friction coefficient was set for the bony endplate-PEEK contact surfaces. (66) The material properties used in the intact and surgical models can be seen in **(Table 1)** To account for age-related degenerative changes in the bony structure, and establish a generalized surgical model, the effects of osteoporosis were modelled through a systematic reduction of the Young's modulus of the bony elements. (53); (54); (55) **(Figure 4)** presents the construction of OLIF models with various fixation options (BPS, LPS, SSA). The FE mesh quality was evaluated by defining the Aspect Ratio (AR) of the volume elements. **(Table 3)** ARs are fundamental metrics used to quantify the geometric configuration of each element within the mesh. Specifically, tetrahedral aspect ratios are determined by the proportion between the longest edge length divided by the minimum altitude of the smallest side. According to the literature: 1<AR<3: acceptable; 3<AR<10: treated with caution, AR>10: treated with alarm. (67); (68)

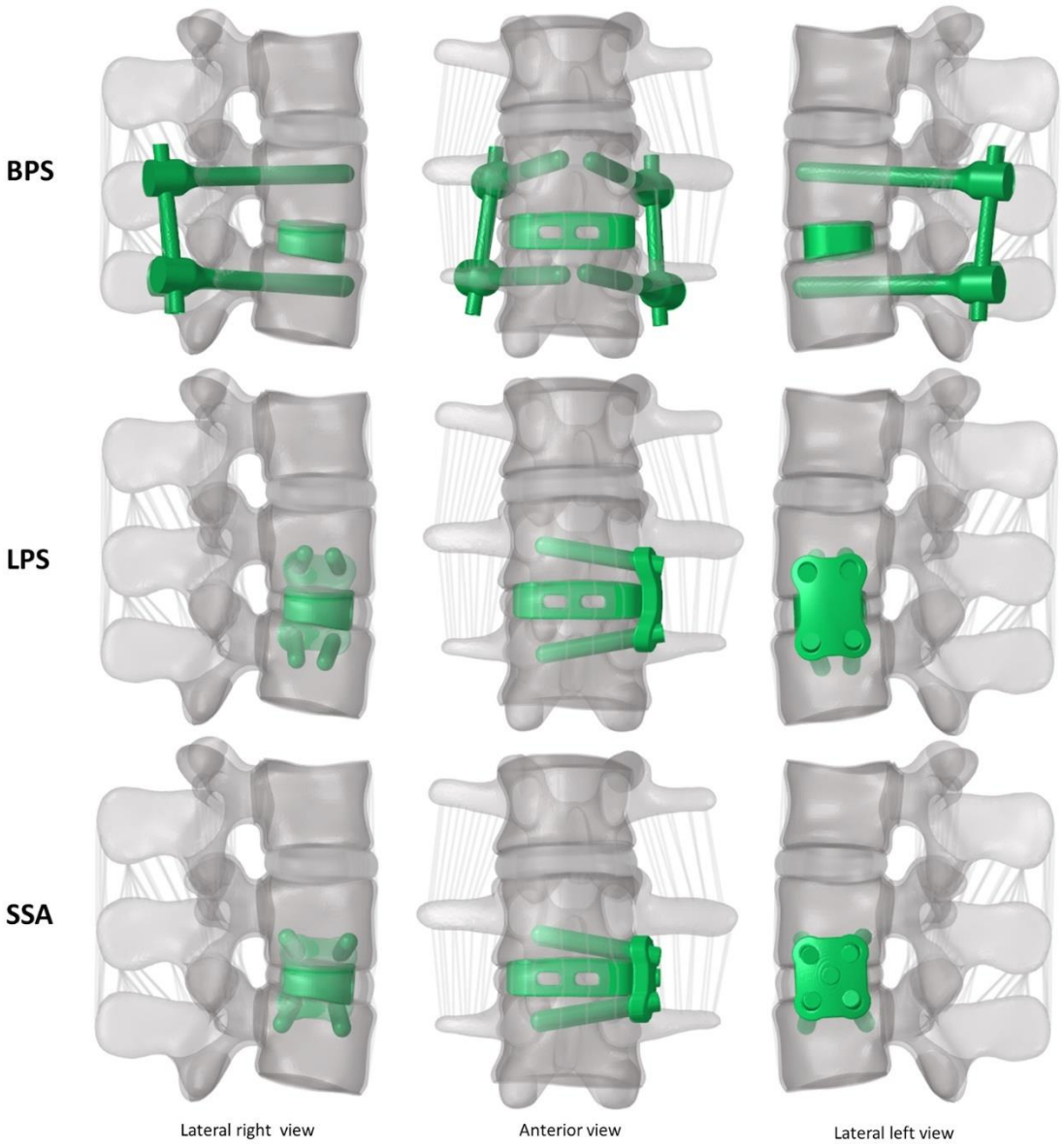

Figure 4. The L2-4 bi-segmental spinal model 3D geometry with the three investigated (OLIF) fixation constructs. **A:** OLIF cage with bilateral pedicle screw (BPS). **B:** OLIF cage with lateral plate-screw (LPS). **C:** self-anchoring stand-alone cage fixation (SSA), lateral left-right, and frontal view.

Material Properties, Boundary and Loading Conditions, FE model validation

The intact L2-4, and the 6 surgical bi-segment FE models (3 normal, and 3 osteoporotic) were exported to Abaqus/CAEv11 (Dassault Systemes, Simulia Corp, Providence, RI, USA) software. Material properties and mesh types assigned to the finite element models are summarized in **(Table 1) and (Table 2)**. In order to validate the created L2-4 intact model, pure 7.5 Nm torque was applied to the L2 vertebral body upper endplate in 3 general directions (flexion-extension, right/left bending, and right/left rotation), while the lower endplate of the L4 vertebra was fixed in place. The intact L2-3 and L3-4 segmental range of motions were compared to a cadaveric study. (69) The lower endplate of the L4 vertebra was fixed in the case of the 6 surgical models as well. The simulations were conducted in 2 steps:

1st step: A 150N Follower Load (FL) was applied between the vertebral bodies. The FL path was defined with the centre of rotation of the vertebrae, hence allowing the load to follow the curvature of the lumbar spine. (70) The study derived from the American Society for the International Association for Testing and Materials (ASTM) 400 N follower load value, to decrease the stabilising effect of trunk muscles, hence highlighting the primary stabilising effect of the implant constructs. The 150 N follower load pattern is widely used in the relevant literature. (28); (71); (72)

2nd step: A pure 10 Nm torque was applied to the L2 vertebral body upper endplate in 3 general directions used for the validation process. (71); (72)

3.2 Part II: Modification of the Validated L2-L4 Bi-segmental Finite Element Model, PMMA Geometry Creation, Finite Element Environment Creation

Development of L2-L4 Lumbar Spinal Bi-segmental Surgical FE Models

The primary objective was to evaluate and compare the impact of PMMA augmentation on the posterior and lateral plate fixation techniques with osteoporotic bony conditions. SSA was chosen for this comparison, hence being the novel implant. To establish the foundation for this study, we employed the previously (in Part I of this thesis) validated intact L2-4 bi-segmental FE model. In addition, the BPS, and SSA surgical FE models were used as well. **(Figure 5)** The 3D simplified intervertebral cage model was remained the same, based on a PEEK (polyether ether ketone) OLIF cage (EMERALD™, Sanatmetal, Eger, Hungary, 45 x 22 x 12 mm, with 6º lordosis) and was inserted from the left side into the L3-4 intervertebral space simulating the surgical process. The same reason was applied when choosing the level of surgery as the previous FE models used in Part I. The L3-4 motion segment provides a surgeon with a comparatively low-risk pathway, where the surgical procedure is seldom impacted by potential interferences from the ascending lumbar vein, the potential upper division of the common iliac vein, or the thoracic cage. (64); (65) Four identical simplified transpedicular screws (5.5x70 mm) (53); (73) were placed inside the L3 and L4 pedicles, and the screwheads were secured with titanium rods to create the BPS construct**.** For the SSA implant, a bi-curved plate (26x23x4 mm) was anchored to the cage with a simplified screw (15x5.5 mm). The plate was affixed to the vertebral bodies with four simplified lateral screws (40x5.5 mm) with diverging axial angles. The material properties applied can be found in Table 1. Osteoporotic bone mineral density was modelled by decreasing Young's modulus of elasticity by a set amount. **(Table 1),** (53); (54); (55) Tie constrains were defined in all bone-implant, PMMA-titanium, and titanium-titanium contact surfaces**.** (26); (74); (75)

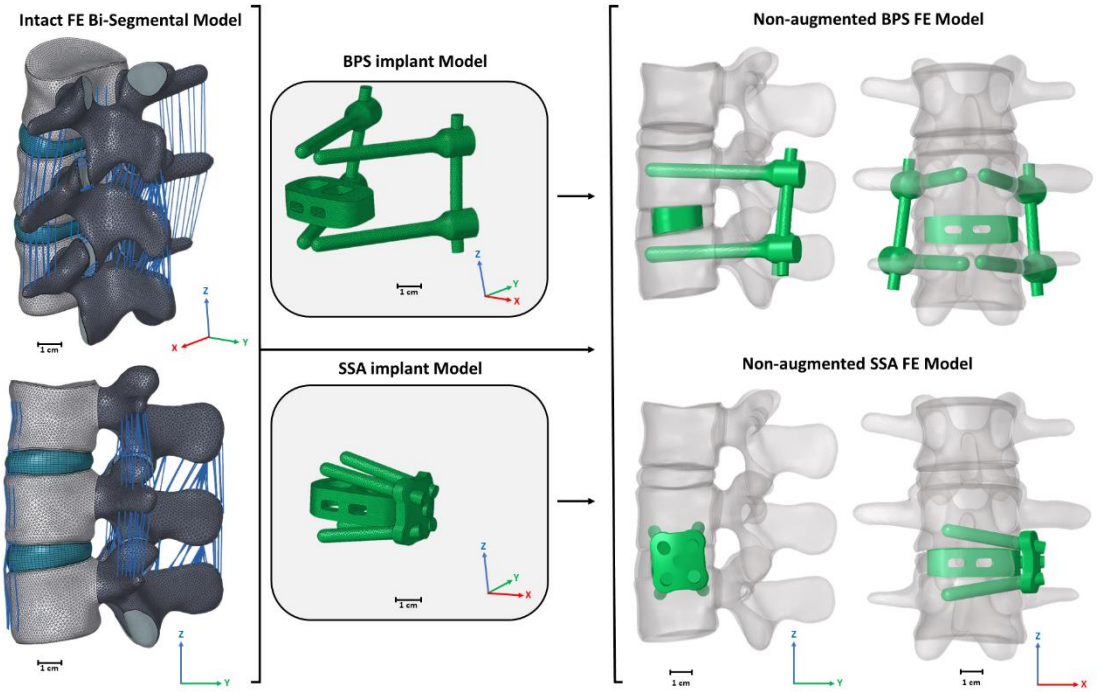

Figure 5. A previously created and validated intact L2-L4 bi-segmental Finite Element (FE) model was used as a base for the surgical constructs. The simplified 3D geometries of the OLIF cage, Bilateral Pedicle Screws (BPS), and Self Anchoring Standalone (SSA) implants were inserted into the intact FE model according to the surgical scenarios, creating the surgical FE geometries without bone cement augmentation.

Model Generation for the PMMA Augmentation

The PMMA augmentation process, utilizing cannulated screws, allows for an infinite variety of shapes and PMMA sizes based on the trabecular structure of the vertebrae**.** (76); (77) To ensure a reproducible simulation environment, uniformly shaped PMMA models were employed. (63); (77) Elongated-spherical-shaped PMMA models were created in Autodesk Fusion 360 (Autodesk Inc., San Rafael, CA, USA) CAD software, using the BPS and SSA screws separately as the base coordinate system for PMMA positioning. The centreline of the PMMA models was aligned to intersect with the screw tips, simulating the augmentation process.

The volume of the created PMMA models were 1 cm^3, 2 cm^3, 3 cm^3, 4 cm^3, 5 cm^3, and 6 cm^3 per screw. The resulting STL files were imported into 3-Matic (Mimics Research, Mimics Innovation Suite v21.0, Materialise, Leuven, Belgium) software. Whenever an intersection between PMMA-PMMA or PMMA-cortical bone was detected, excess PMMA was removed (for PMMA-PMMA: Boolean union; for PMMA–Cortical bone: Boolean subtraction), and the remaining PMMA mass was adjusted to retain the original volume using the Push and Pull tool, performed by two experienced spinal surgeons. The final augmented PMMA geometries can be observed in **(Figure 6).**

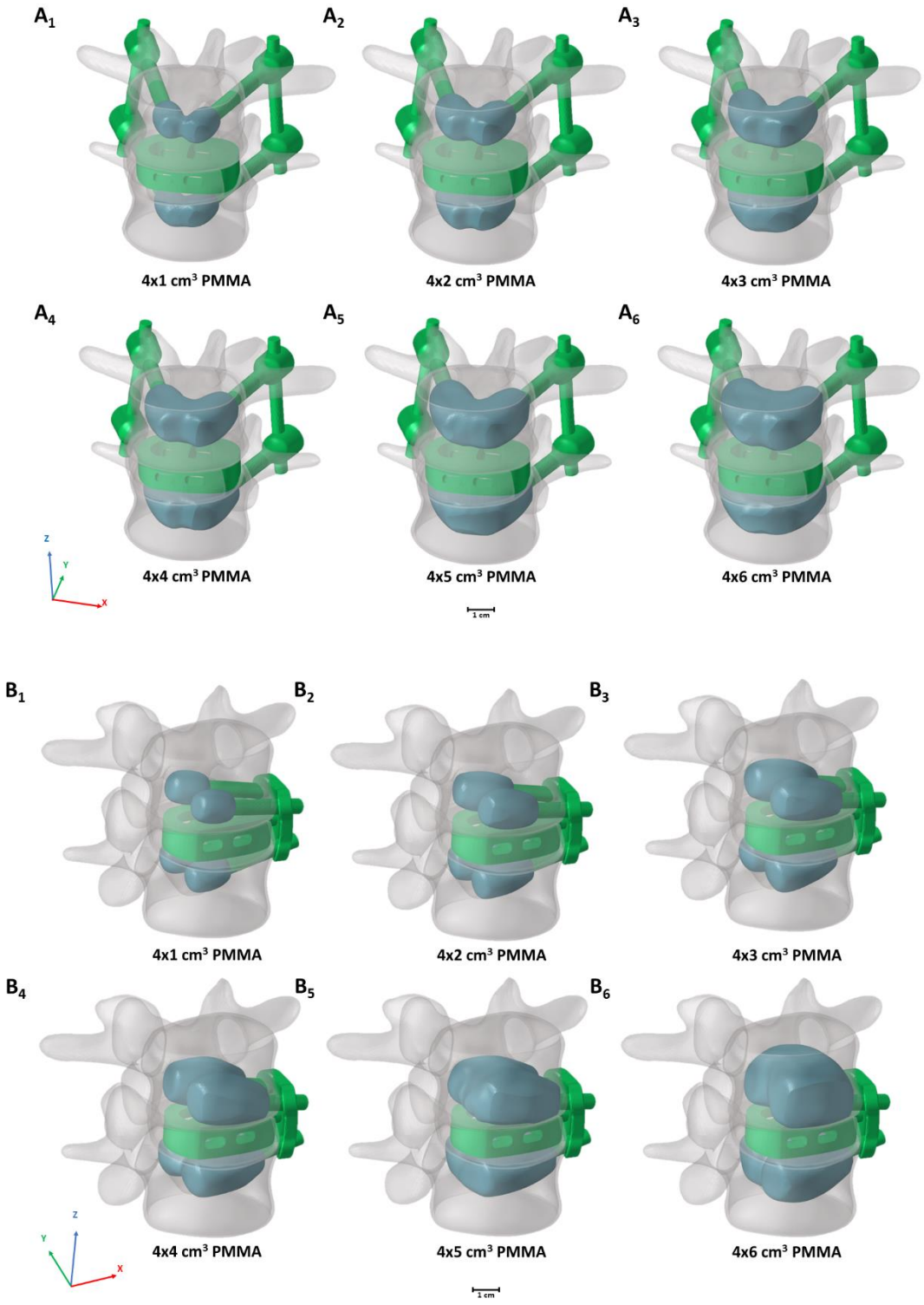

Figure 6. The two surgical Finite Element (FE) model constructs investigated with gradually increasing volumes of injected PMMA per screw. **A1-A6:** Bilateral Pedicle Screw (BPS) constructs. **B1-B6:** Self Anchoring Standalone (SSA) constructs.

Boundary and Loading Conditions

A total of 16 FE models were created: BPS and SSA implants with normal bone (2 FE models), BPS and SSA with osteoporotic bone (2 FE models), and the 6-6 gradually increasing augmented models with osteoporosis from 1 cm^3 to 6 cm^3 (12 FE models) **(Figure 6).** FE model assembly and further modifications were conducted using HyperWorks software (Altair Engineering, Inc., Troy, Michigan, USA). The finalized FE models were exported to Abaqus/CAEv11 (Dassault Systemes, Simulia Corp, Providence, RI, USA) for the simulation processes. All FE simulations were performed in two consecutive steps. First, a 400 N follower load was applied through the middle of the vertebral bodies. Second, a bending moment of 10 Nm was applied to the superior endplate of the L2 vertebral body in the three anatomical planes to simulate flexion, extension, left-right lateral bending, and left-right axial rotation**.** (78)**;** (79) The inferior endplate of L4 was fixed in all degrees of freedom during the simulations. Following the ASTM standard 400 N follower load was applied to the investigated constructs, so the implants could be tested with higher trunk muscle loads, adding more variables to the simulations done in Part I of this thesis.

4. RESULTS

4.1. Part I

Model Validation

In order to evaluate the accuracy of the L2-L4 segmentation process, two investigators created the 3D geometries of the L2-L4 bony structures separately. The DSI quantifies the relative volume overlap between two segmentations. The obtained DSI value for the vertebras was 94 %, indicating a high accuracy of the segmented models. (80) The FE mesh quality was evaluated by defining the Aspect Ratio (AR) of the volume elements **(Table 3)** (67); (68) 98,4 % of the elements' ARs building up the anatomical parts of the FE mesh were between 1 and 3, and 99,85% of the elements' ARs building up the implants of the FE mesh were between 1 and 3 (1<AR<3), which is the acceptable margin. Only 1,6% of the anatomical element's ARs, and 0,15 % of the implants element's ARs was between 3 and 10 (3<AR<10), which is still adequate for FE simulation, but needs to be treated with caution. (67); (68) None of the FE elements' ARs exceeded the 10 AR mark.

The results of the Range of Motion (ROM) values were in accordance with the findings of previous cadaveric study by Ilharreborde et al. 2011. (69) **(Figure 7)** The ROM of L2-3 motion segment in flexion-extension, lateral bending, axial rotation was 5.86°, 9.01°, and 4.59° respectively. In the cadaveric experiment, the corresponding ROM of L2-3 was 6.8°±2.5°, 7.3°±2.3°, and 4.7°±2.7°. For the L3-4 segment the ROM for flexion-extension, lateral bending, and axial rotation was 6.19°, 7.92°, 4.72° in our model, and 6.6°±3.5°, 7.9°±4.5°, and 5.5°±3.9° for the cadaveric experiment.

The ROM comparison results suggested that the intact L2-4 FE model in the present study was successfully constructed and could be used for further investigation.

Table 3. The calculated Aspect Ratio (AR) of the volume elements building up the finite element mesh. According to the literature: 1<AR<3: acceptable; 3<AR<10: treated with caution, AR>10: treated with alarm. ST: Stand Alone; LP: Lateral Plate.

Level	Parts	Element number	1<AR<3	%	3<AR<10	%	10<AR	%
L2	Cortical bone	15182	15149	99,78	33	0,22	0	0
	Trabecular bone	47612	47602	99,98	10	0,02	0	0
	Bony endplates	28225	24909	88,25	3316	11,75	0	0
	Post. elements	379801	378421	99,64	1380	0,36	0	0
	Facet joints	35317	35317	100,00	0	0,00	0	0
L3	Cortical bone	18169	18143	99,86	26	0,14	0	0
	Trabecular bone	47264	47264	100,00	0	0,00	0	0
	Bony endplates	20147	18444	91,55	1703	8,45	0	0
	Post. elements	490942	490526	99,92	416	0,08	0	0
	Facet joints	46430	46430	100,00	0	0,00	0	0
L4	Cortical bone	16444	16373	99,57	71	0,43	0	0
	Trabecular bone	54631	54587	99,92	44	0,08	0	0
	Bony endplates	30845	28583	92,67	2262	7,33	0	0
	Post. elements	564319	562549	99,69	1770	0,31	0	0
	Facet joints	53032	53032	100,00	0	0,00	0	0
L2-3	Cartilage endplates	3542	3538	99,89	4	0,11	0	0
	Nucleus	11470	11427	99,63	43	0,37	0	0
	Annulus	6240	6240	100,00	0	0,00	0	0
L3-4	Cartilage endplates	3744	3612	96,47	132	3,53	0	0
	Nucleus	12600	12552	99,62	48	0,38	0	0
	Annulus	6120	6120	100,00	0	0,00	0	0
Implant								
CAGE		123722	123612	99,91	110	0,09	0	0
GRAFT		71856	71758	99,86	98	0,14	0	0
PLATE_SA		48794	48708	99,82	86	0,18	0	0
PLATE_LP		59321	59126	99,67	195	0,33	0	0
POST_SCREW		151603	151581	99,99	22	0,01	0	0

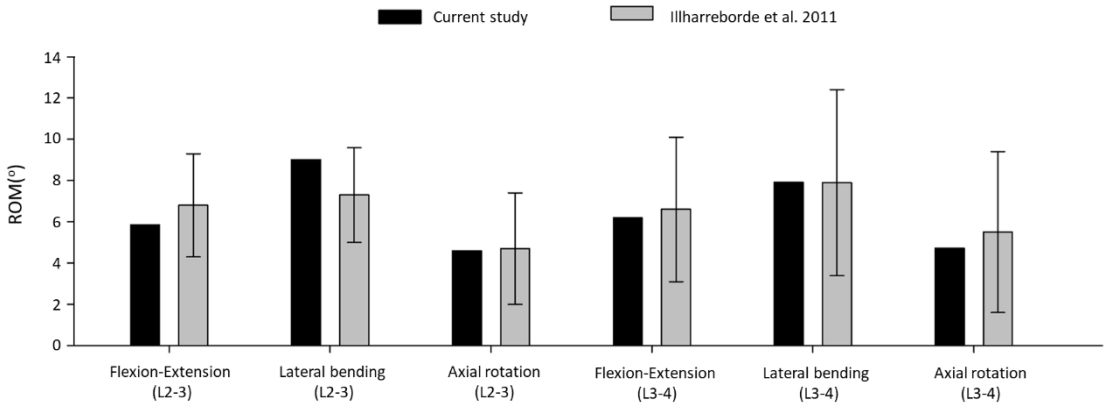

Figure 7. Comparison of the computed range of motions given by the intact L2-L4 bi-segmental model with experimental results for 7.5 Nm pure moments.

ROM, Displacement and Cortical Endplate Stress Distribution

In order to compare the primary stabilising properties of the 3 investigated implants, the ROMs of the virtually operated motion segments were compared. To evaluate the interaction between the inserted cage and the bony endplate below it, the cage's caudal displacement, and the endplate's surface stress distribution was investigated. Additionally, osteoporosis induced L4 screw displacement increase was studied to better understand which implant's screws are the least affected by the osteoporosis. A total of 6 surgical constructs were modelled and analysed, corresponding to the BPS, LPS, SSA fixation options with normal and osteoporotic bone material property. The ROM of the surgical models under a combined loading of 150 N follower load and 10 Nm torque is shown in **(Figure 8A)**. After the OLIF cage was inserted, the predicted ROM at the surgical level (L3-L4) decreased in all motion conditions compared with the intact model **(Figure 7); (Figure 8A)**. Osteoporosis increased the ROM in all directions compared to the normal bone material property models. The highest impact caused by osteoporosis on the ROM occurred in the LPS fixation construct, where the ROM increased by 97.3% in flexion, 86.3% in extension, 30.14% in left bending, 140.26% in right bending, 50.96% in left rotation and 53.38% in right rotation.

The BPS provided the most stable fixation with low ROM values in normal and porotic conditions with the exception of the right bending scenario. The highest difference between the BPS and lateral plate systems (LPS, SSA) was found in the left and right-side rotation. For normal bone the difference in BPS vs LPS was 99%, BPS vs SSA was 119.73 %, and for the porotic bone BPS vs LPS was 158.94%, BPS vs SSA was 145.49%.

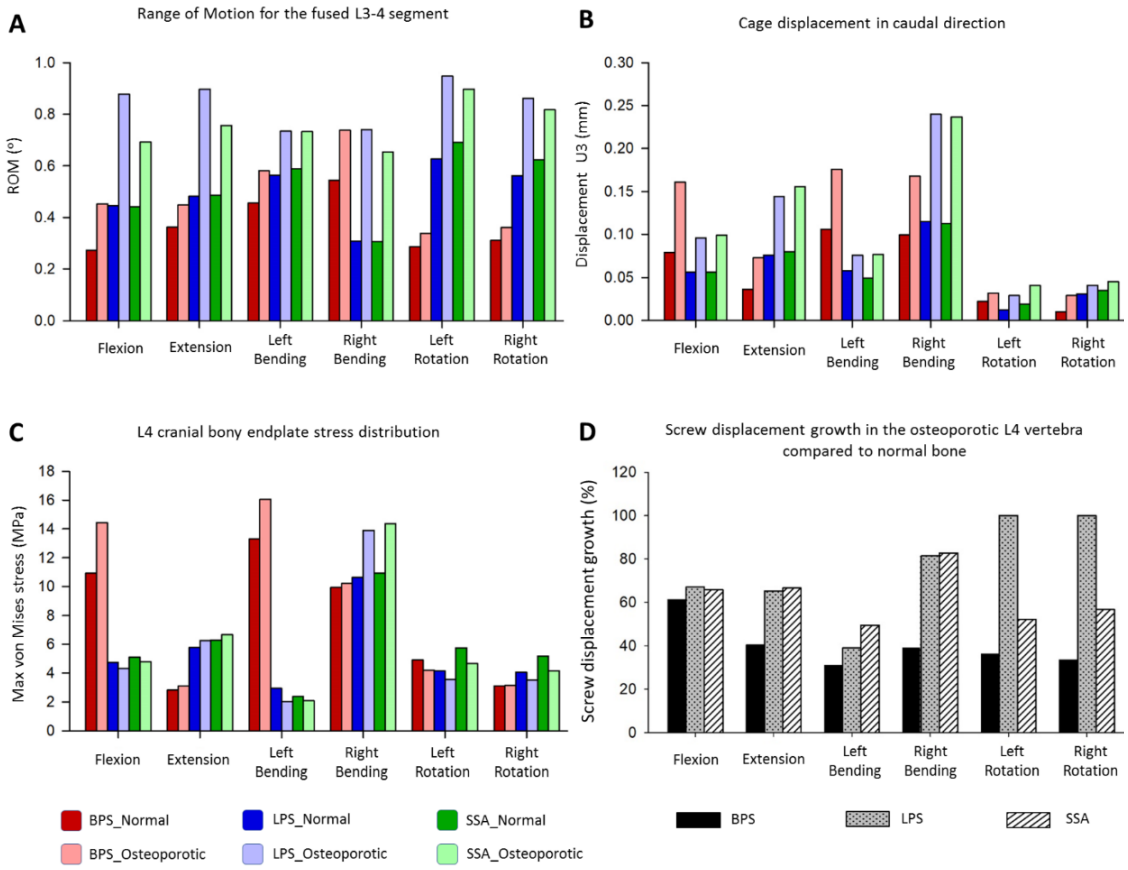

Figure 8. Results of the simulations extracted from the surgically reconstructed bi-segmental FEA model according to the six loading scenarios in normal and osteoporotic condition. **A:** range of motion (ROM) values for the operated L3-4 segment containing the investigated implants constructs (BPS: bilateral pedicle screw, LPS: lateral plate-screw, SSA: self-anchored standalone). **B:** cage displacement in the caudal direction (U3 in Abaqus). **C:** Von Mises stress peaks on the L4 cranial bony endplate. **D:** The measured L4 screw displacement increase (%) caused by osteoporotic bony conditions compared to L4 screw displacements inside normal bone.

Osteoporosis increased the cage displacement in caudal direction (U3) for all of the fixation constructs **(Figure 8B); (Figure 9).** The highest increase in displacement was found in right bending for the LPS (from 0.115 mm to 0.24 mm, 109%), and for the SSA (from 0.113 mm to 0.237 mm, 110%). With the exception for flexion and left bending, the BPS fixation had lower displacement values both for normal and osteoporotic condition compared to LPS and SSA. Overall, the cage displacement values were similar for the SSA and LPS.

The von Mises stress peaks on the L4 upper cortical endplate are shown in **(Figure 8C).** Compared to normal bone, the stress peaks increased in the osteoporotic models for extension, right bending and right rotation. In flexion and left bending the stress peaks for the BPS model were much higher compared to the other models (LPS, SSA) regardless of the bone material properties (Von Mises peaks for BPS were 10.92 MPa and 13.31 MPa for flexion and left bending in normal bone and 14.43 MPa and 16.06 MPa in osteoporotic condition). To investigate this phenomenon the von Mises stress distribution on the L4 upper cortical endplates were visualised using contour plots **(Figure 10).** This showed that the exceling von Mises stress peaks in flexion and left bending for the BPS models are stress concentrations at the place of the fenestration of the anulus fibrosus and the OLIF cage border.

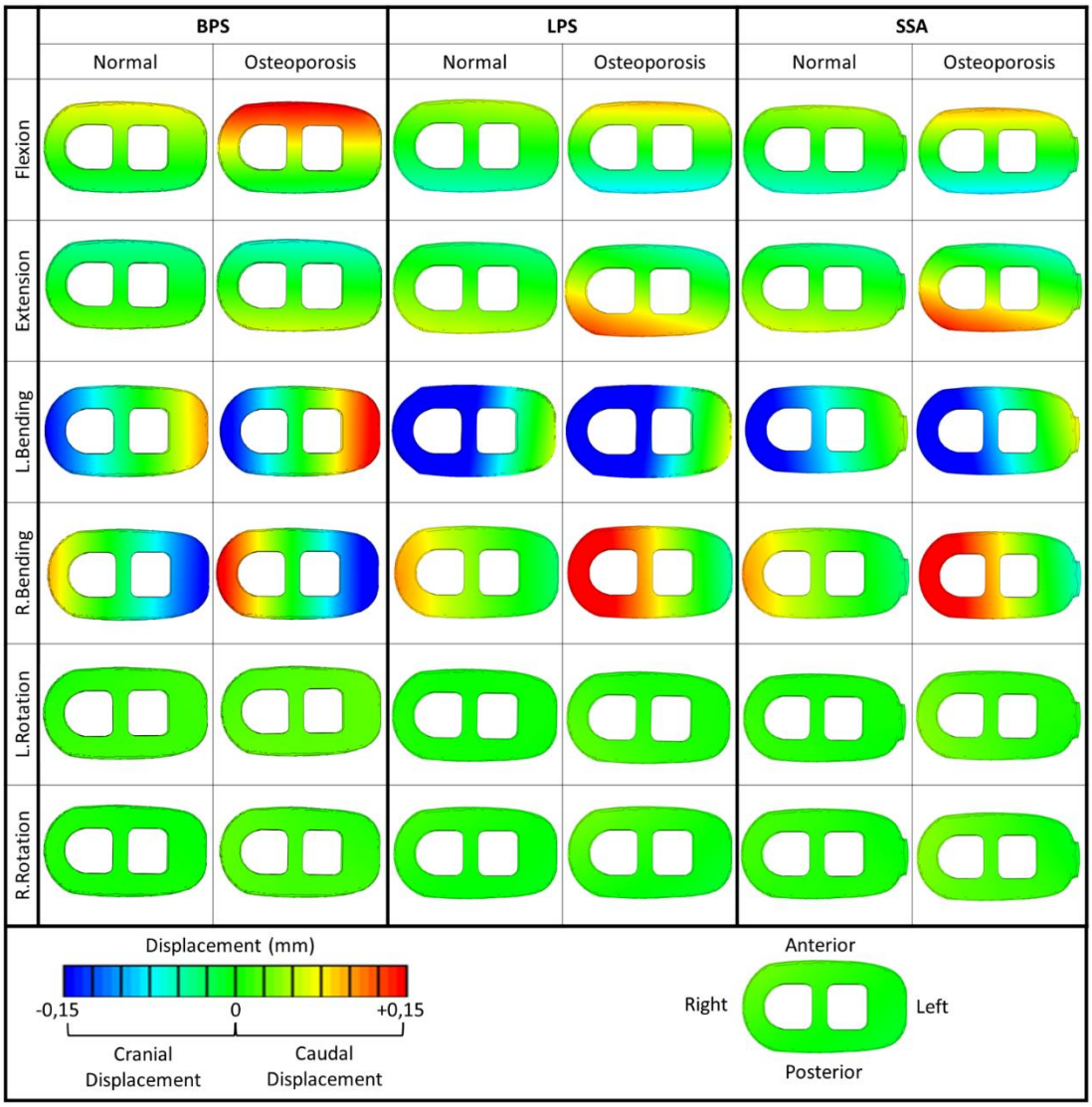

Figure 9. Color map of the cage displacements (U3) in the cranio-caudal direction in the three OLIF models with various fixation options (BPS: bilateral pedicle screw, LPS: lateral plate-screw, SSA: self-anchored standalone) in normal and osteoporotic bone material property condition. Displacement is represented by the Colorbar (Blue/Green/Red), scale: -0.15–0.15 mm, bottom view

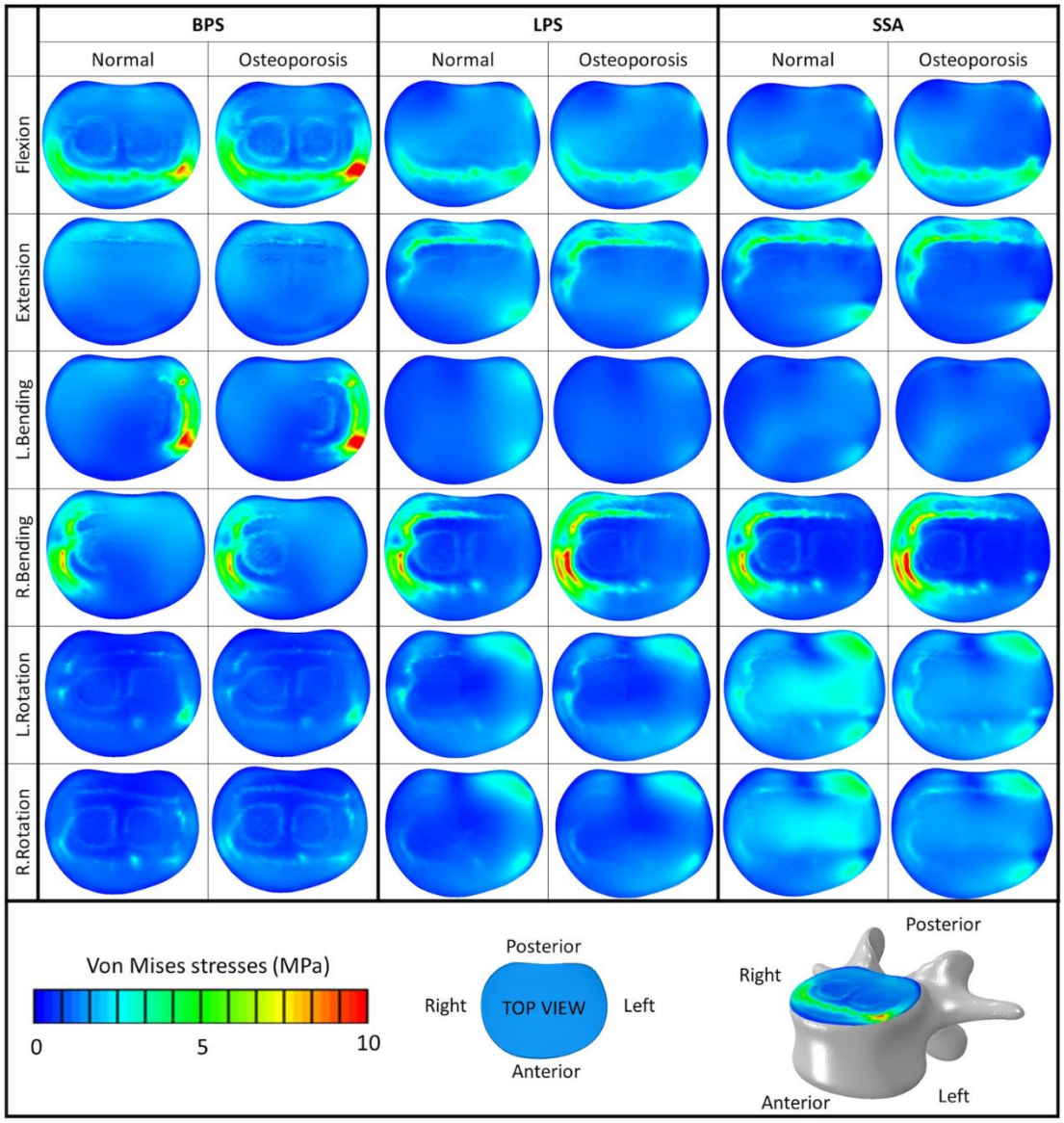

Figure 10. Von Mises stress distribution on the cranial bony endplate of the L4 vertebra, with various fixation option (BPS: bilateral pedicle screw, LPS: lateral plate-screw, SSA: self-anchored standalone) in normal and osteoporotic condition under six loading loading scenarios. Colorbar (Blue/Green/Red), scale (0-10 MPa), top view.

The screw displacement was measured by highlighting the screw tips inside the L4 vertebra in the 3 constructs. The distance between two points were measured: Point 1: screw tip location before applying the forces. Point 2: screw tip location after the last "step" (Step is a basic concept in Abaqus FE solver software) (81) of the simulation in a direction, and the result was the average of the 2 values (always 2 screws inside the L4).

The osteoporosis increased the screw displacement in the L4 vertebra in all motion conditions compared to the normal bone models **(Figure 8D).** The highest increase was found in the case of LPS fixation for left (100%) and right (100%) rotation. The impact of osteoporosis on the BPS fixation screw displacement was lower in all of the 6 general modelled motions, compared to the other two implants. (screw displacement increase in BPS model for flexion: 61.38%, extension: 40.38%, left bending: 31%, right bending: 39%, left rotation: 36.32 %, right rotation: 33.48%, For the LPS model 67,2% in flexion, 65,21% in extension, 39,2 % in left bending, 81,35% in right bending, 100% in left rotation, 100% in right rotation. For the SSA model 65,82% in flexion, 66,66% in extension, 49,48 % in left bending, 82,81% in right bending, 52,17% in left rotation, 56,71% in right rotation)

4.2. Part II

L3-4 Segmental Range of Motion

The measured L3-L4 segmental Range of Motion (ROM) values under the combined loading of a 400 N follower load and a 10 Nm bending moment are displayed in **(Figure 11).** In normal bone conditions, except for left bending, the BPS system exhibited smaller ROM values. Due to osteoporosis, the segmental ROM was increased in all six bending moments for both investigated implants, amplifying the existing difference between them. These values align with the result from Part I (150N follower load). PMMA augmentation gradually reduced the ROM in both BPS and SSA constructs with osteoporotic bone. At 3 cm^3 of injected PMMA per screw (half of the investigated maximum amount), the segmental ROM values for BPS decreased by 27.3% in flexion, 10.5% in extension, 13.0% in right bending, 6.3% in left bending, 11.4% in right rotation, and 7.5% in left rotation compared to the non-augmented osteoporotic ROM values. For SSA. the values decreased by 41.3% in flexion, 49.1% in extension, 61.9% in right bending, 30.3% in left bending, 41.9% in right rotation, and 36.7% in left rotation.

At 6 cm^3 of injected PMMA volume per screw, compared to the non-augmented values the ROM decrease for BPS was 34.2% in flexion, 12.8% in extension, 24.4% in right bending, 17.1% in left bending, 21.4% in right rotation, and 14.9% in left rotation. For

SSA, the values were decreased by 65.3% in flexion, 68.9% in extension, 75.6% in right bending, 44.5% in left bending, 58.4% in right rotation, and 54.9% in left rotation. Compared to the non-augmented ROM values in osteoporosis, at 6 cm^3 injected PMMA volume per screw, the difference between the two implants reduced by 25.9% in flexion, 98.3% in extension, 36.5% in right bending, 62.9% in right rotation, and 76.5% in left rotation. Only in left bending, the difference increased between SSA and BPS by 23.0%.

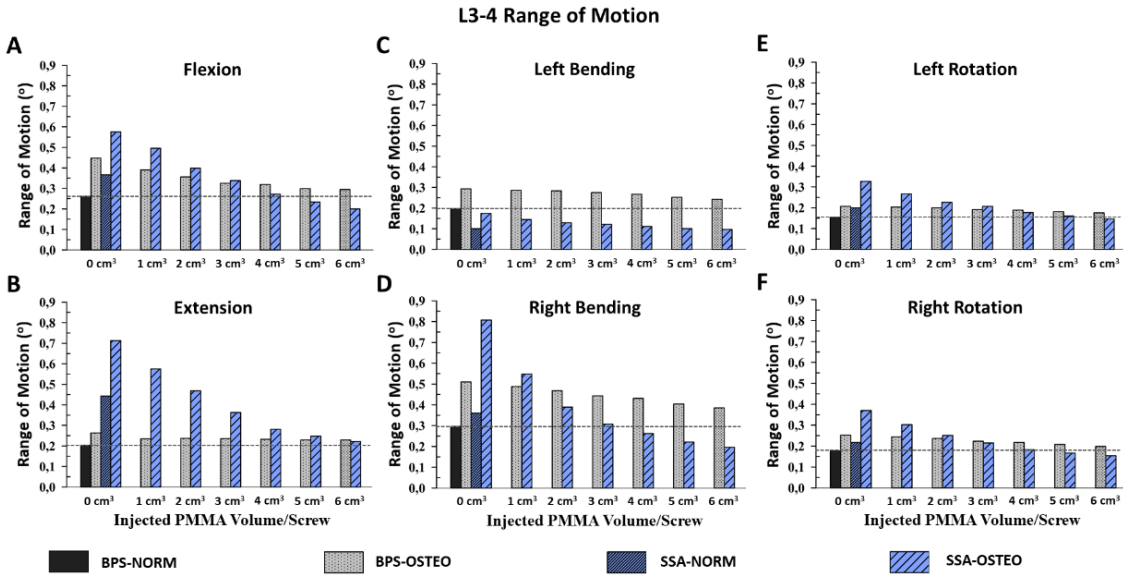

Figure 11. Range of motion values for operated L3-L4 segments in the 6 investigated bending moments visualized with grouped bar charts. The values on the y-axis are in degrees (°), and the values on the x-axis for all the graphs are in cubic centimetres (cm^3). BPS-NORM: Bi-Pedicle Screws + normal bone; BPS-OSTEO: Bi-Pedicle Screws + osteoporotic bone; SSA-NORM: Self-anchoring Stand-Alone + normal bone; SSA-OSTEO: Self-anchoring Stand-Alone + osteoporotic bone. The horizontal line represents the BPS-NORM values.

OLIF Cage Caudal Displacement

The inserted OLIF cage's maximal caudal displacement values at the end of each simulation are presented in **(Figure 12).** In normal bone conditions, the BPS system had smaller values compared to the SSA system, except for left bending, and flexion. Osteoporosis increased the displacement values in both of the investigated constructs, further increasing the existing difference between BPS and SSA constructs. PMMA augmentation in osteoporotic bone gradually reduced the displacement values in both of

the implants. At 3 cm^3 of injected PMMA volume per screw (half of the investigated maximum amount), the cage's caudal displacement values for BPS decreased by 61.5% in flexion, 13.2% in extension, 31.9% in right bending, 18.9% in left bending, 28.7% in right rotation, and 54.2% in left rotation compared to the non-augmented osteoporotic caudal displacement values. For SSA, the values were decreased by 35.2% in flexion, 43.9% in extension, 58.3% in right bending, 3.0% in left bending, 66.5% in right rotation, and 66.1% in left rotation.

At 6 cm^3 of injected PMMA volume per screw, compared to the non-augmented values, the cage's caudal displacement decreases for BPS was 71.5% in flexion, 59.0% in extension, 59.0% in right bending, 35.7% in left bending, 60.2% in right rotation, and 67.8% in left rotation. For SSA, the values were decreased by 62.4% in flexion, 58.8% in extension, 73.2% in right bending, 11.7% in left bending, 80.7% in right rotation, and 81.7% in left rotation.

Compared to the non-augmented values in osteoporosis, at 6 cm^3 injected PMMA per screw, the difference in the cage's caudal displacement values between the two implants reduced considerably: 49.0% reduction in flexion, 76.0% in extension, 96.8% in right bending, 48.6% in left bending, 89.9% in right rotation, 96.7% in left rotation. At higher amounts of injected PMMA, SSA had smaller values in left bending and both rotational movements, while BPS had smaller values in flexion, extension, and right bending.

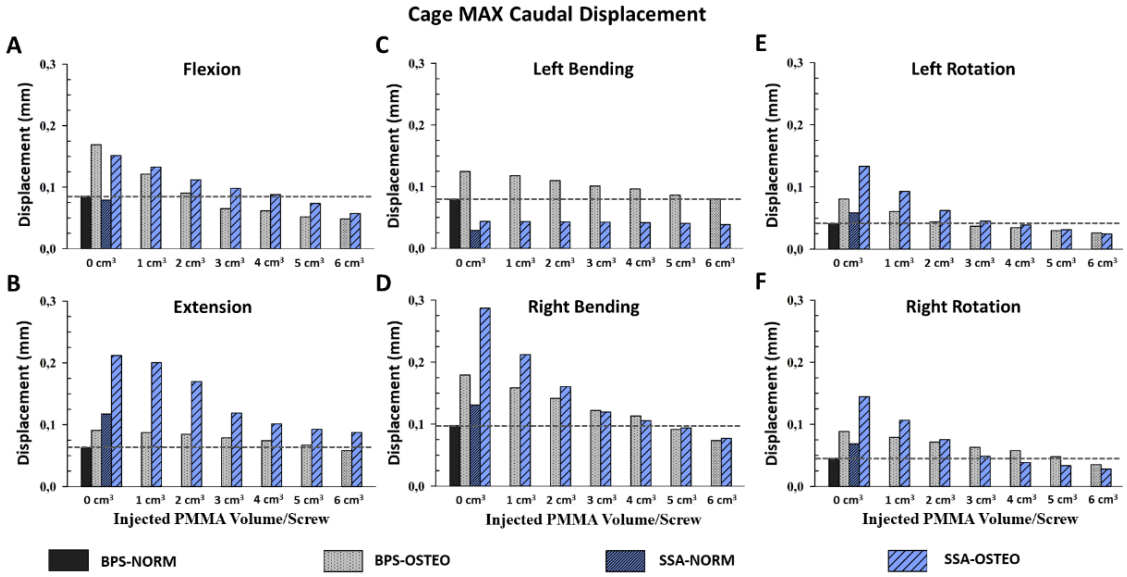

Figure 12. Maximal caudal displacement values of the inserted cage visualized with grouped bar charts. The values on the y-axis are in millimetres (mm), and the values on the x-axis for all the graphs are in cubic centimetres (cm^3). BPS-NORM: Bi-Pedicle Screws + normal bone; BPS-OSTEO: Bi-Pedicle Screws + osteoporotic bone; SSA-NORM: Self-anchoring Stand-Alone + normal bone; SSA-OSTEO: Self-anchoring Stand-Alone + osteoporotic bone. The horizontal line represents the BPS-NORM values.

Principal Stress on the Cranial Endplate of L4 Vertebra

The maximal Principal Stress values at the end of each bending cycle can be observed in **(Figure 13).** The results are similar to the previous two investigated values (ROM and displacement), with the injected PMMA reducing the maximal stress values on the endplate directly below the cage. The largest stress peak was observed in the SSA system during right bending (17.8 MPa), significantly increased by osteoporosis (25.2 MPa). This value in osteoporosis at 3 cm^3 PMMA augmentation is decreased by 54.4%, at 6 cm^3 by 71%. At 3 cm^3 of injected PMMA volume per screw (half of the investigated maximum amount), the maximal L4 endplate Principal Stress values for BPS decreased by 59.9% in flexion, 15.0% in extension, 37.4% in right bending, 32.2% in left bending, 48.8% in right rotation, and 10.3% in left rotation compared to the non-augmented osteoporotic values.

For SSA, the values decreased by 45.1% in flexion, 44.8% in extension, 54.4% in right bending, 24.9% in left bending, 45.8% in right rotation, and 46.8% in left rotation.

At 6 cm^3 of injected PMMA volume per screw, compared to the non-augmented values, the L4 endplate Principal Stress values for BPS decreased by 76.4% in flexion, 38.2% in extension, 59.4% in right bending, 55.9% in left bending, 63.5% in right rotation, and 36.4% in left rotation. For SSA, the values decreased by 60.9% in flexion, 60.7% in extension, 71.0% in right bending, 49.7% in left bending, 66.1% in right rotation, and 68.8% in left rotation.

Compared to the non-augmented values in osteoporosis, at 6 cm^3 injected PMMA per screw, the difference in the endplate stress values between the two implants reduced considerably: 95.2% reduction in flexion, 81.2% in extension, 86.7% in right bending, 57.4% in left bending, 83.1% in left rotation. Except for right rotation, where the difference increased (45.2% increase). However, the values in this scenario are relatively close to each other, so the high percentage can be misleading. For the non-augmented BPS model, the maximal stress was 15.3 MPa, while for SSA, it was 15.2 MPa. After the 6 cm^3 per screw augmentation, the value for BPS was 5.6 MPa, and 5.2 MPa for SSA.

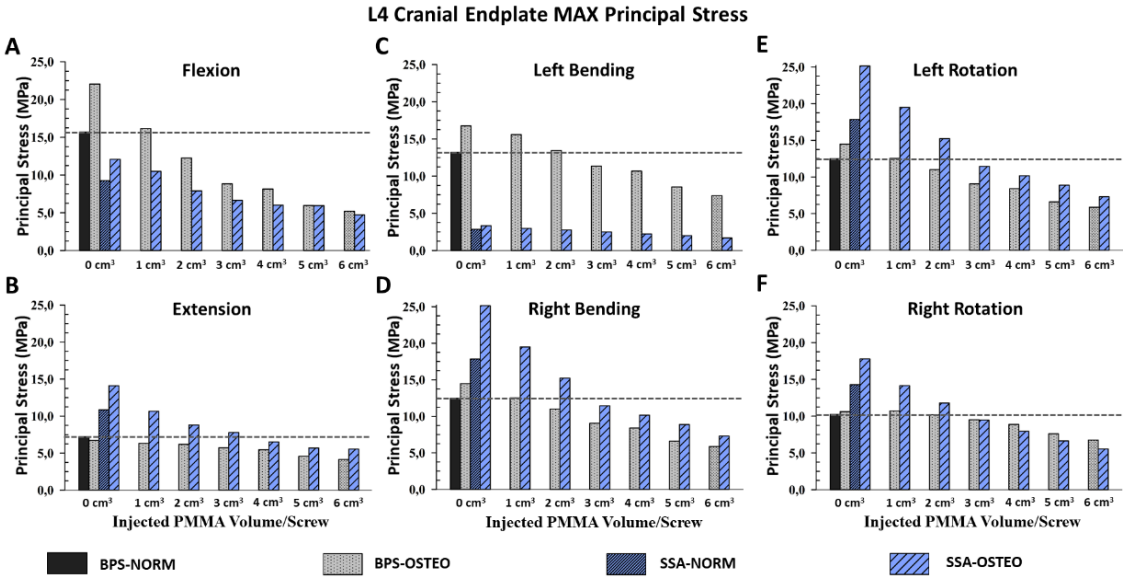

Figure 13. Maximal principal stress values alongside the L4 cranial endplate below the inserted cage visualized with grouped-bar charts. The values on the y-axis are in megapascal (MPa), and the values on the x-axis for all the graphs are in cubic centimeters (cm^3). BPS-NORM: Bi-Pedicle Screws + normal bone; BPS-OSTEO: Bi-Pedicle Screws + osteoporotic bone; SSA-NORM: Self-anchoring Stand-Alone + normal bone; SSA-OSTEO: Self-anchoring Stand-Alone + osteoporotic bone. The horizontal line represents the BPS-NORM values.

5. DISCUSSION

5.1. Part I

Primary Stability of the OLIF Implants with Normal, and Osteoporotic Bony Conditions.

In the past decade due to the advancement in minimally invasive spinal fusion technologies, (17) the OLIF procedure have emerged and it has been used more often by spine surgeons. The advantages of OLIF surgical technique includes: preservation of the posterior structures of the lumbar spine, reduced blood loss and shorter hospital stay. (21) Despite the fact that OLIF has been successfully adopted in the clinical environment, the risks of cage subsidence and screw loosening are possible postoperative complications related to this technique. (82) Biomechanical failure of the stabilization construct (cage subsidence, loosening of the screws) is a multifactorial phenomenon (damage to endplates during preparation, over distraction, cage design, etc.) (82) Bone quality as well as the biomechanical stability of the whole fusion construct can have a significant role in the development of this complication, possibly influencing the short- and long-term therapeutic outcome. Part I of this thesis aimed to investigate the effect of bone quality on the stability of a fused segment with the aid of FEA models in 3 different fixation options.

First, the intact L2-4 bi-segment FE model was developed and validated by comparing the ROMs (ante- retroflexion, lateral-flexion, rotation) under pure 7.5 Nm torque to the findings of a previous cadaveric study by Ilharreborde et al. (69) The adequate validation results **(Figure 7)** allowed us to take a step further and modify the FE model to establish the different OLIF construct models: BPS, LPS, SSA, with normal and osteoporotic bone material properties **(Figure 4).**

The ROM of the surgical models under a combined loading of 150 N follower load and 10 Nm torque **(Figure 8A)** showed different behaviours based on the fixation type and the bone material property (normal/osteoporotic). BPS provided the most stable fixation in both normal and osteoporotic conditions. These findings were in accordance with Guo et al**.** (28) who used a L3-5 bi-segment FE model to evaluate OLIF constructs with various fixation options under the same combined loading of 150 N and 10 Nm.

They applied normal bone material property and found similar result for the ROMs and that BPS provides the highest stability compared to lateral only fixations.

The recent publication by Song et al. (79) represents the pioneering effort in utilizing Finite Element (FE) models to construct an osteoporotic spinal model (L1-S1) in order to investigate the biomechanical stability of the OLIF procedure with multiple fixation methodologies specifically within the scope of a single-segment (L3-4). They found a similar trend in the results, that BPS provides a more stable fixation than lateral plates in normal and osteoporotic condition despite the differences between their (boundary conditions, axial compressive preload of 400 N, and torsional moment of 10 Nm) and our models. Song's lateral plate fixation design concept differed from the model presented in this thesis (the lateral plate was fixed to the vertebral body with 2 screws in their model, while 4 screws were used in our constructs), and his investigation did not include the self-anchored standalone OLIF cage concept. Based on the results osteoporosis increased the ROM in all motion conditions compared to the normal bone material property models. The highest impact caused by osteoporosis on ROM occurred in the LPS fixation construct. The highest difference between the BPS and lateral plate systems (LPS, SSA) was found in rotational movements.

Osteoporosis increased the cage displacement in caudal direction (U3 in Abaqus) for all of the fixation options **(Figure 8B).** Overall, the cage displacement values were similar for the SSA and LPS systems. The highest increase in displacement was found in right bending for the LPS, and for the SSA implants. With the exception for flexion, and left bending BPS fixation had lower displacement values both for normal and osteoporotic condition. Parallelly to the caudal displacement the opposite side of the cages can move to the cranial direction **(Figure 9).** The complex mechanism of subsidence involving the upper and lower endplates supported by radiological findings is still widely investigated. (82)

Compared to normal bone, in the osteoporotic models have got increased values for the von Mises stress peaks on the L4 upper cortical endplate **(Figure 8C)** for extension, right bending, and right rotation. In flexion and left bending the BPS model values were much higher compared to the other models (LPS, SSA) regardless of the bone material properties. Stress concentrations at the place of the anulus fibrosus fenestration and the OLIF cage border occurred in BPS model in flexion and left bending**. (Figure 10)**

In the other loading scenarios higher stresses can be observed on the endplate surface for the LPS and SSA models compared to the BPS model. Song's study found that on the investigated L4 endplate, the stress values increase with osteoporosis but it is lower for the BPS implants compared to lateral plate fixation (79)

Osteoporosis increased the screw displacement values in the L4 vertebra in all motion conditions compared to normal bone models **(Figure 8D).** The highest increase was found in the case of LPS fixation for left (100 %) and right (100 %) rotation. The impact of osteoporosis on the BPS fixation screw displacement was lower in all of the 6 general modelled motions compared to the other fixations.

The results of Part I of this thesis highlight that the possible advantages of the LPS, SSA fixation (e.g. lower operation time and invasiveness due of the lack of the posterior – percutaneous – fixation steps) can be hindered in osteoporotic patients. In osteoporotic patients the BPS provides a more stable fixation than LPS, SSA what is important to avoid mechanical complications and provide optimal therapeutic outcome.

Limitations of Part I

Although the FE analysis has many advantages over in vitro experiments, it has limitations as well, e.g. its inability to "perfectly" mimic the human tissue mechanics. In order to simulate certain biomechanical processes inside the human body, simplifications need to be made due to the limitations of in silico software's. Osteoporosis, and normal bone quality is not uniformly distributed among the human skeleton. There can be vertebras, and regions inside the vertebras that are more affected by osteoporosis and can lead to weaker spots. This line of thought leads to an infinite amount of bone mechanical quality distribution models, so in this thesis the path of creating a uniform bone material model for our investigations were chosen. The osteoporosis FE model was constructed by decreasing the elastic modulus of the normal uniform cortical and cancellous bone by a certain proportion. However in the literature more complex approaches are described to model osteoporosis, by integrating micro-level trabecular structural mechanics. (83) With ageing, degenerative changes are occurring in the spine not only affecting the vertebral bone material property but the geometry, (exp. stabilising osteophytes) (84) and the internal structure of the intervertebral disc as well. Therefore, in an osteoporotic model, the non-surgically treated discs, and bony structures should be altered accordingly.

In this thesis the osteoporotic model had the same bony geometry and intervertebral disc material property as the normal bony model.

The developed model investigated the primary stability of the constructs right after the surgery, not taking in consideration the expected fusion process, because long term bony fusion is often the desired result of an adequately chosen implant and correctly executed surgery.

5.2. Part II

Stability Evaluation of the Modified FE OLIF Constructs, with Normal and Osteoporotic Bony Conditions

In summary, a total of 16 FE OLIF surgical models were analysed. BPS and SSA constructs in normal and osteoporotic bony conditions without any PMMA augmentation. In osteoporosis, the two implants were investigated with gradually increasing volumes of PMMA augmentation per screw (ranging from 1 cm^3 to 6 cm^3) under the combined loading of a 400 N follower load and a 10 Nm bending moment. To assess the stability of the operated motion segments and the implants, segmental ROM values **(Figure 11),** the inserted OLIF cage's caudal displacement values **(Figure 12**), and the L4 upper endplate stress values **(Figure 13)** were compared between the two implant constructs. Based on the results, the BPS system provides greater primary stability compared to the SSA construct, and this difference is further increased by osteoporosis. These findings align with the results from Part I of this thesis, the existing literature, which has investigated similar, albeit slightly different boundary and loading conditions**.** (26)**;** (27)**;** (79) In normal bony conditions, BPS exhibited smaller ROM values, except for left bending. The positioning of the plate on the left side of the vertebral bodies may explain its increased resistance to left bending moments, which is reflected in the results. The difference between the two implants becomes more pronounced in osteoporosis **(Figure 11).** One of the possible complications associated with lumbar spinal fusion surgeries is cage subsidence into the caudal, or cranial vertebral body through an endplate defect. (85) In a recently published systematic review by Parisien et al. the median incidence of such a complication in OLIF surgery with posterior fixation ranged from 4.4% to 36.9%. (86)

According to the literature, cage subsidence displays a proclivity to occur at the endplate situated beneath the inserted cage. (87); (88); (89) To estimate the likelihood of this complication, we measured the inserted OLIF cage's maximum caudal displacement values, and the L4 upper endplate stress values directly below the cage at the end of each bending cycle**.** (90)**;** (91) In normal bone, except for flexion and left bending, the BPS system exhibited smaller displacement, and stress values, compared to the SSA construct, and these differences were further magnified by osteoporosis **(Figure 12); (Figure 13).** In the case of flexion, the compressive forces are concentrated on the anterior part of the vertebral body, requiring the cage to bear most of these forces. In extension, the BPS construct's posterior screw-rod system takes over part of the compression forces from the cage. These results align with previous finite element-assisted studies of TLIF surgeries, where the stress values of the cage and the endplate below it were greater in flexion compared to extension, while the stress values on the posterior screws were higher in extension compared to flexion. (66); (92) This may explain the higher BPS values in flexion.

The Effect of PMMA Augmentation on the Constructs' Biomechanical Stability

In the elderly population, osteoporosis can contribute to substantial morbidity and mortality**.** (93) This condition poses a challenge to spine surgeons, as osteoporotic bone cannot provide a stable anchoring point for screws and offers less resistance against the compression forces from the implants. (94) PMMA, first used by Charnley et al. in the 1960s for total joint replacement in orthopaedic surgery (95) has since been adapted for various spinal surgical procedures. The primary goal of PMMA screw augmentation is to create a better anchoring point for the screws to increase implant stability. (96) Screw pullout strength and the effect of PMMA on screw loosening have been extensively investigated in the literature. (32); (33); (96) However, there is a lack of published articles on the effect of PMMA augmentation on the overall stability of the operated motion segment, particularly with implants used in OLIF surgeries.

In osteoporotic bone, the two implants (BPS, SSA) were investigated with gradually increasing volumes of PMMA augmentation per screw (ranging from 1 cm^3 to 6 cm^3). In the case of the BPS construct, PMMA augmentation gradually reduced the segmental ROM, the cage's caudal displacement, and L4 upper endplate stress values**. (Figure 11); (Figure 12); (Figure 13).** The most significant effect of augmentation on ROM was observed in flexion, with a decrease of 27.3% at 3 cm^3, and 34.2% at 6 cm^3. Flexion was also one of the most affected attributes for cage caudal displacement (61.5% decrease at 3 cm^3 and 71.5% at 6 cm^3) and L4 upper endplate stress values (59.5% decrease at 3 cm^3 and 76.4% at 6 cm^3). These results are favourable, considering the higher average stress values in posterior fixation constructs discussed earlier**.** (66); (92)

Similar results were observed with the SSA construct, as the gradually increasing volumes of augmented PMMA led to gradual reductions in the investigated values. As seen in the results **(Figure 11),** the less stable non-augmented SSA construct was more affected by augmentation than the BPS construct. When summarizing the results for the six investigated bending moments, the mean ROM decrease at 3 cm^3 of PMMA augmentation was 12.7% for BPS and 43.5% for SSA, and at 6 cm^3 of PMMA, it was 20.8% for BPS and 61.3% for SSA. The summarized decrease in the cage's maximum caudal displacement values at 3 cm^3 of PMMA augmentation was 34.7% for BPS and 45.5% for SSA, and at 6 cm^3 of PMMA, it was 55.0% for BPS and 61.4% for SSA. The summarized values for L4 maximum upper endplate stress at 3 cm^3 of PMMA augmentation were a 33.9% decrease for BPS and 43.6% for SSA, and at 6 cm^3 of PMMA, it was 55.0% for BPS and 62.9% for SSA.

As observed in the results section, the difference between the investigated values of the BPS and SSA constructs gradually decreased with increasing amounts of PMMA augmented inside the vertebral bodies, making the two implants biomechanically comparable in osteoporotic bone. At 6 cm^3 of PMMA augmentation per screw, the mean decrease in the differences was 60% in ROM (excluding left bending), 75.7% in the cage's maximal caudal displacement, and 80.7% in the L4 upper endplate maximal stress values (excluding right rotation).

Minimally invasive spine surgery has become increasingly popular in the last decade due to its goal of minimizing surgical morbidity, and recent technological advancements**.** (97)

Studies have reported faster operative times, fewer adverse reactions, and quicker returns to work. (98); (99) For older, more frail populations, the use of minimally invasive methods, such as the SSA construct in OLIF surgery, are advantageous (18) as it eliminates the need for patient repositioning and additional incisions and can be performed through the original incision. However, it comes at the cost of offering inferior primary stability compared to the BPS construct in osteoporosis as can be seen in Part I of this thesis, and the relevant literature**.** (26)**;** (27)**;** (28) As demonstrated in **(Figure 11); (Figure 12); (Figure 13)** the SSA construct can achieve the primary stability of the non-augmented BPS construct in osteoporotic bone, with PMMA augmentation. The SSA ROM values became smaller in osteoporosis compared to the non-augmented BPS values after 2 cm^3 PMMA augmentation per screw in flexion, 5 cm^3 in extension, 2 cm^3 in right bending, 3 cm^3 in right rotation, and 3 cm^3 in left rotation. For the cage's maximal displacement values, the SSA required 5 cm^3 of PMMA augmentation per screw in extension, 2 cm^3 in right bending, 2 cm^3 in right rotation, and 2 cm^3 in left rotation. The values for L4 endplate maximal stresses are 4 cm^3 PMMA augmentation volume per screw in extension, 3 cm^3 in right bending, and 3 cm^3 in left rotation. For right bending, the results for the two implants were relatively similar. The average of the results obtained for the three investigated parameters (ROM, cage caudal displacement, L4 upper endplate stress) comes between 3 cm^3 and 4 cm^3 PMMA per screw.

However, PMMA screw augmentation is not without its limitations and potential complications. In a recent meta-analysis done by Zhang et. al. (100) regarding the complication rates associated with screw augmentation, by far the most prevalent complication was cement leakage at 21.8%. Symptomatic leakage, which potentially required revision surgery, occurred in 1.6% of cases. Other factors included screw loosening (2%), pulmonary embolism (3%), adjacent compression fractures (3.1%), and infections (3%). To reduce the risk of cement leakage, high-viscosity cements can be used with promising results. (101); (102) The incidence of leakage can also be associated with greater amounts of bone cement injected. (103) Therefore, one possible approach to reduce the risk of leakage is to use smaller amounts of PMMA, while attempting to achieve adequate biomechanical stability. Based on our results, it appears that between 3 cm^3 and 4 cm^3 of injected PMMA per screw could be an adequate amount for the SSA construct to reach the primary stability of the non-augmented BPS construct.

Limitations of Part II

Despite its many advantages over in vitro experiments, finite element (FE) analysis also has limitations that prevent it from precisely replicating human tissue mechanics. To tackle biomechanical processes within the human body, certain simplifications must be made due to the constraints of in silico software. Within the human skeleton, osteoporotic and normal bone qualities are not uniformly distributed, resulting in regions within the vertebrae that are subsequently weaker. Furthermore, the geometry of these regions, such as the presence of stabilizing osteophytes, may undergo changes with aging. Additionally, the internal structure of intervertebral discs also undergoes alterations. This complexity results in an infinite number of bone material property distribution models, so a uniform bone material model was created for the FE simulations. The effect of implants on the whole lumbar spine cannot be investigated, as this FE model incorporates only 2 motion segments from the lumbar spine. The FE model used in this study is unable to accurately predict the fatigue strength of the implants due to the static load and the simplified implant geometries. The model also does not consider the effect of lordosis, and the effect of stabilisation on adjacent intervertebral discs of the operated motion segment. Despite the aforementioned limitations, the presented FE model was able to offer a direct biomechanical comparison between the two investigated implants, and the effect of PMMA augmentation with osteoporotic bony conditions. The model could be developed further by adding additional spinal motion segments including the sacral bone, and test multiple levels of OLIF surgery, which could be used in further biomechanical testing.

6. CONCLUSIONS

The aging population in developed countries presents an ongoing challenge for spine surgeons due to decreased bone quality, and comorbidities. Minimally invasive surgery can be a solution for this frail population, but it has drawbacks. A review of the relevant literature revealed a lack of consensus on the optimal fixation options for OLIF surgeries in older population, creating a demand/clinical problem (Needs Finding Stage in Stanford Biodesign process). Based on the results of Part I of this thesis bilateral pedicle screw (BPS) and rod fixation provided superior biomechanical stability for OLIF cages, compared to self-anchored standalone (SSA) or lateral plate-screw fixated (LPS) cages both in normal and osteoporotic conditions. The osteoporosis amplified the difference between the stability of the bilateral pedicle screw fixation and the two other investigated fixation methods. Clinically, in the case of decreased bone quality (primary or secondary osteoporosis), the surgeon has to take into consideration the limits of the SSA and LPS, despite the advantage that there is no need for a second step in the surgery by turning the patient to prone position to perform the percutaneous pedicle screw fixation.

Part II of this thesis aimed to investigate the effect of PMMA augmentation on the BPS, and SSA constructs. Based on the results, PMMA augmentation can improve stability in both constructs, narrowing the gap between them. It is important to note that increasing the volume of injected PMMA raises the risk of leakage. The research suggests that injecting between 3 cm^3 and 4 cm^3 of PMMA per screw can achieve comparable stability to the BPS system in the SSA construct. Currently, there is no consensus-based guideline on when to use PMMA augmentation in OLIF surgery or the appropriate amount to inject, and further biomechanical studies are required to understand the effects and risks of PMMA augmentation. According to the results of the study and the clinical need, the concept of an SSA augmentation device is desirable but currently not available on the market. These findings suggest opportunities for continued research, potential advancements/innovations, and the development of new products for the marketplace. (Concept Generation/Screening Stage in Stanford Biodesign process)

7. SUMMARY (1PAGE)

The objective of this doctoral thesis was to conduct computerized in silico simulations to investigate the different implant constructs used in OLIF surgeries. Specifically, the focus was on comparing the two-step surgery required posterior fixation constructs (BPS) with the one-step surgery lateral plate systems (SSA, LPS) in normal and osteoporotic conditions. Additionally, the thesis aimed to determine if the use of PMMA augmentation could enhance primary stability and minimize differences between OLIF constructs in osteoporotic bone. The research was conducted in two parts.

In Part I of the thesis a spinal bi-segmental L2-4 finite element model was created, and validated based on the literature. The model was further modified to represent the presence of osteoporosis. Simplified 3D implant models used in OLIF surgeries were successfully incorporated into the L3-4 motion segment during a virtual surgical procedure, resulting in surgical finite element models. A two-step simulation method was employed, involving a follower-load followed by bending and rotational movements. Primary stability was assessed through four parameters: ROM of the operated segment, caudal displacement of the OLIF cage, maximum stress concentration on the endplate beneath the cage, and increased screw motion induced by osteoporosis. The results indicated that BPS provided superior biomechanical stability for OLIF cages compared to SSA or LPS constructs, under both normal and osteoporotic conditions. Furthermore, osteoporosis exacerbated the difference in the primary stability between the bilateral pedicle screw fixation and the two other investigated fixation methods.

In Part II of the thesis, the impact of PMMA augmentation on osteoporotic bone was examined for BPS and the novel SSA implant constructs. Surgical models with PMMA augmentation were created, with the amount of injected PMMA/screw gradually increasing from 1 cm^3 to 6 cm^3. The simulation method used was similar to that used in Part I. ROM, caudal displacement of the cage, and maximum stress concentrations on the endplate beneath the cage were investigated. The findings revealed that PMMA augmentation can enhance stability in both constructs, thereby reducing the existing disparity between them. The research suggests that injecting between 3 cm^3 and 4 cm^3 of PMMA per screw can achieve comparable stability to the BPS system in the SSA construct. Based on the findings, the concept of an SSA augmentation device is desirable but currently not available on the market.

8. REFERENCES

1. Huiskes R, Chao EYS. A survey of finite element analysis in orthopedic biomechanics: The first decade. J Biomech. 1983;16:385–409. doi: 10.1016/0021-9290(83)90072-6. Cited: in: : PMID: 6352706.
2. Carniel EL, Fontanella CG, Polese L, Merigliano S, Natali AN. Computational tools for the analysis of mechanical functionality of gastrointestinal structures. Technol Heal Care. 2013;21:271–283. doi: 10.3233/THC-130722. Cited: in: : PMID: 23792800.
3. Carniel EL, Toniolo I, Fontanella CG. Computational Biomechanics: In-Silico Tools for the Investigation of Surgical Procedures and Devices. Bioengineering. 2020;7:48. doi: 10.3390/bioengineering7020048.
4. Zhou C, Cha T, Wang W, Guo R, Li G. Investigation of Alterations in the Lumbar Disc Biomechanics at the Adjacent Segments After Spinal Fusion Using a Combined In Vivo and In Silico Approach. Ann Biomed Eng. 2021;49:601–616. doi: 10.1007/s10439-020-02588-9. Cited: in: : PMID: 32785861.
5. Zander T, Dreischarf M, Schmidt H, Bergmann G, Rohlmann A. Spinal loads as influenced by external loads: A combined in vivo and in silico investigation. J Biomech. 2015;48:578–584. doi: 10.1016/j.jbiomech.2015.01.011. Cited: in: : PMID: 25648494.
6. Viceconti M, Henney A, Morley-Fletcher E. In silico clinical trials: how computer simulation will transform the biomedical industry. Int J Clin Trials. 2016;3:37. doi: 10.18203/2349-3259.ijct20161408.
7. Welch-Phillips A, Gibbons D, Ahern DP, Butler JS. What Is Finite Element Analysis? Clin Spine Surg A Spine Publ. 2020;33:323–324. doi: 10.1097/BSD.0000000000001050.
8. Brekelmans WA, Poort HW, Slooff TJ. A new method to analyse the mechanical behaviour of skeletal parts. Acta Orthop Scand. 1972;43:301–317. doi: 10.3109/17453677208998949. Cited: in: : PMID: 4651051.
9. Ye Y, You W, Zhu W, Cui J, Chen K, Wang D. The Applications of Finite Element Analysis in Proximal Humeral Fractures. Comput Math Methods Med. 2017;2017. doi: 10.1155/2017/4879836. Cited: in: : PMID: 29081829.
10. Goel VK, Nyman E. Computational Modeling and Finite Element Analysis. Spine

(Phila Pa 1976). 2016;41:S6–S7. doi: 10.1097/BRS.0000000000001421.

11. Wieding J, Souffrant R, Mittelmeier W, Bader R. Finite element analysis on the biomechanical stability of open porous titanium scaffolds for large segmental bone defects under physiological load conditions. Med Eng Phys. 2013;35:422–432. doi: 10.1016/j.medengphy.2012.06.006. Cited: in: : PMID: 22809675.
12. Naoum S, Vasiliadis A V., Koutserimpas C, Mylonakis N, Kotsapas M, Katakalos K. Finite Element Method for the Evaluation of the Human Spine: A Literature Overview. J Funct Biomater. 2021;12:43. doi: 10.3390/jfb12030043.
13. Mobbs RJ, Phan K, Malham G, et al., Seex K, Rao PJ. Lumbar interbody fusion: techniques, indications and comparison of interbody fusion options including PLIF, TLIF, MI-TLIF, OLIF/ATP, LLIF and ALIF. J spine Surg. 2015;1:2. doi: 10.3978/j.issn.2414-469X.2015.10.05. Cited: in: : PMID: 27683674.
14. Resnick DK, Choudhri TF, Dailey AT, Groff MW, Khoo L, Matz PG, Mummaneni P, Watters WC, Wang J, Walters BC. Guidelines for the performance of fusion procedures for degenerative disease of the lumbar spine. Part 7: intractable low-back pain without stenosis or spondylolisthesis. J Neurosurg Spine. 2005;2:670–672.
15. Fuster V. Changing Demographics: A New Approach to Global Health Care Due to the Aging Population. J. Am. Coll. Cardiol. Elsevier USA; 2017. p. 3002–3005. Available from: http://www.news.va/en/.
16. Fehlings MG, Tetreault L, Nater A, Choma T, Harrop J, Mroz T, Santaguida C, Smith JS. The aging of the global population: the changing epidemiology of disease and spinal disorders. Neurosurgery. 2015;77:S1–S5.
17. Yue JJ, Guyer R, Johnson JP, Khoo LT, Hochschuler SH. The Comprehensive Treatment of the Aging Spine E-Book: Minimally Invasive and Advanced Techniques-Expert Consult. Elsevier Health Sciences; 2010.
18. Shamji MF, Goldstein CL, Wang M, Uribe JS, Fehlings MG. Minimally invasive spinal surgery in the elderly: does it make sense? Neurosurgery. 2015;77:S108–S115.
19. Mayer MH. A New Microsurgical Technique for Minimally Invasive Anterior Lumbar Interbody Fusion1996 Scientific Program Committee. Spine (Phila Pa 1976). 1997;22.

20. Silvestre C, Mac-Thiong J-MM, Hilmi R, Roussouly P. Complications and Morbidities of Mini-open Anterior Retroperitoneal Lumbar Interbody Fusion: Oblique Lumbar Interbody Fusion in 179 Patients. Asian Spine J. 2012/05/31. 2012;6:89–97. doi: 10.4184/asj.2012.6.2.89.
21. Phan K, Maharaj M, Assem Y, Mobbs RJ. Review of early clinical results and complications associated with oblique lumbar interbody fusion (OLIF). J Clin Neurosci. 2016;31:23–29. doi: 10.1016/j.jocn.2016.02.030. Cited: in: : PMID: 27349468.
22. Mehren C, Mayer HM, Zandanell C, Siepe CJ, Korge A. The oblique anterolateral approach to the lumbar spine provides access to the lumbar spine with few early complications. Clin Orthop Relat Res. 2016;474:2020–2027. doi: 10.1007/s11999-016-4883-3. Cited: in: : PMID: 27160744.
23. Chung N-S, Jeon C-H, Lee H-D, Kweon H-J. Preoperative evaluation of left common iliac vein in oblique lateral interbody fusion at L5–S1. Eur Spine J. 2017;26:2797–2803.
24. Li R, Li X, Zhou H, Jiang W. Development and Application of Oblique Lumbar Interbody Fusion. Orthop Surg. 2020;12:355–365. doi: 10.1111/os.12625.
25. Kim H, Chang BS, Chang SY. Pearls and Pitfalls of Oblique Lateral Interbody Fusion: A Comprehensive Narrative Review. Neurospine. Korean Spinal Neurosurgery Society; 2022. p. 163–176. Available from: /pmc/articles/PMC8987540/.
26. Cai XY, Bian HM, Chen C, Ma XL, Yang Q. Biomechanical study of oblique lumbar interbody fusion (OLIF) augmented with different types of instrumentation: a finite element analysis. J Orthop Surg Res. 2022;17:269. doi: 10.1186/s13018-022-03143-z. Cited: in: : PMID: 35568923.
27. Liu ZX, Gao ZW, Chen C, Liu ZY, Cai XY, Ren YN, Sun X, Ma XL, Du CF, Yang Q. Effects of osteoporosis on the biomechanics of various supplemental fixations co-applied with oblique lumbar interbody fusion (OLIF): a finite element analysis. BMC Musculoskelet Disord. 2022;23:1–12. doi: 10.1186/s12891-022-05645-7. Cited: in: : PMID: 35986271.
28. Guo H-Z zhi, Tang Y-C chao, Guo D-Q qing, Luo P-J jie, Li Y-X xian, Mo G-Y ye, Ma Y-H huai, Peng J-C cheng, Liang D, Zhang S-C cong. Stability Evaluation

of Oblique Lumbar Interbody Fusion Constructs with Various Fixation Options: A Finite Element Analysis Based on Three-Dimensional Scanning Models. World Neurosurg. 2020;138:e530–e538. doi: 10.1016/j.wneu.2020.02.180. Cited: in: : PMID: 32156592.

29. Sozen T, Ozisik L, Calik Basaran N. An overview and management of osteoporosis. Eur J Rheumatol. 2017;4:46–56. doi: 10.5152/eurjrheum.2016.048.
30. Weiser L, Huber G, Sellenschloh K, Viezens L, Püschel K, Morlock MM, Lehmann W. Insufficient stability of pedicle screws in osteoporotic vertebrae: biomechanical correlation of bone mineral density and pedicle screw fixation strength. Eur Spine J. 2017;26:2891–2897. doi: 10.1007/s00586-017-5091-x. Cited: in: : PMID: 28391382.
31. Wang W, Liu C, Li J, Li H, Wu J, Liu H, Li C, Zhou Y. Comparison of the fenestrated pedicle screw and conventional pedicle screw in minimally percutaneous fixation for the treatment of spondylolisthesis with osteoporotic spine. Clin Neurol Neurosurg. 2019;183:105377. doi: 10.1016/j.clineuro.2019.105377. Cited: in: : PMID: 31279300.
32. Bostelmann R, Keiler A, Steiger HJ, Scholz A, Cornelius JF, Schmoelz W. Effect of augmentation techniques on the failure of pedicle screws under cranio-caudal cyclic loading. Eur Spine J. 2017;26:181–188. doi: 10.1007/s00586-015-3904-3. Cited: in: : PMID: 25813011.
33. Becker S, Chavanne A, Spitaler R, Kropik K, Aigner N, Ogon M, Redl H. Assessment of different screw augmentation techniques and screw designs in osteoporotic spines. Eur Spine J. 2008;17:1462–1469. doi: 10.1007/s00586-008-0769-8. Cited: in: : PMID: 18781342.
34. Martín-Fernández M, López-Herradón A, Piñera AR, Tomé-Bermejo F, Duart JM, Vlad MD, Rodríguez-Arguisjuela MG, Alvarez-Galovich L. Potential risks of using cement-augmented screws for spinal fusion in patients with low bone quality. Spine J. 2017;17:1192–1199. doi: 10.1016/j.spinee.2017.04.029. Cited: in: : PMID: 28606606.
35. Janssen I, Ryang YM, Gempt J, Bette S, Gerhardt J, Kirschke JS, Meyer B. Risk of cement leakage and pulmonary embolism by bone cement-augmented pedicle screw fixation of the thoracolumbar spine. Spine J. 2017;17:837–844. doi:

10.1016/j.spinee.2017.01.009. Cited: in: : PMID: 28108403.

36. Hoppe S, Keel MJB. Pedicle screw augmentation in osteoporotic spine: indications, limitations and technical aspects. Eur J Trauma Emerg Surg. 2017;43:3–8. doi: 10.1007/s00068-016-0750-x. Cited: in: : PMID: 27995283.
37. Combley R. Cambridge business English dictionary. Cambridge University Press; 2011.
38. Maranville S. Entrepreneurship in the Business Curriculum. J Educ Bus. 1992;68:27–31. doi: 10.1080/08832323.1992.10117582.
39. Wall J, Wynne E, Krummel T. Biodesign process and culture to enable pediatric medical technology innovation. Semin Pediatr Surg. 2015;24:102–106. doi: 10.1053/j.sempedsurg.2015.02.005. Cited: in: : PMID: 25976143.
40. Yock PG, Brinton TJ, Zenios SA. Teaching biomedical technology innovation as a discipline. Sci. Transl. Med. American Association for the Advancement of Science; 2011. Available from: https://www.science.org.
41. Castro-Mateos I, Pozo JM, Lazary A, Frangi A. 3D Vertebra segmentation by feature selection active shape model. Recent Adv Comput methods Clin Appl spine imaging. Springer; 2015. p. 241–245.
42. Rijsbergen M van, van Rietbergen B, Barthelemy V, Eltes P, Lazáry Á, Lacroix D, Noailly J, Ho Ba Tho M-C, Wilson W, Ito K. Comparison of patient-specific computational models vs. clinical follow-up, for adjacent segment disc degeneration and bone remodelling after spinal fusion. PLoS One. 2018;13:e0200899. doi: 10.1371/journal.pone.0200899. Cited: in: : PMID: 30161138.
43. Aryanto KYEE, Oudkerk M, van Ooijen PMAA. Free DICOM de-identification tools in clinical research: functioning and safety of patient privacy. Eur Radiol. 2015;25:3685–3695. doi: 10.1007/s00330-015-3794-0. Cited: in: : PMID: 26037716.
44. Zou KH, Warfield SK, Bharatha A, Tempany CMC, Kaus MR, Haker SJ, Wells WM, Jolesz FA, Kikinis R. Statistical Validation of Image Segmentation Quality Based on a Spatial Overlap Index. Acad Radiol. 2004;11:178–189. doi: 10.1016/S1076-6332(03)00671-8. Cited: in: : PMID: 14974593.
45. Bharatha A, Hirose M, Hata N, Warfield SK, Ferrant M, Zou KH, Suarez-Santana

E, Ruiz-Alzola J, D'Amico A, Cormack RA, et al. Evaluation of three-dimensional finite element-based deformable registration of pre- and intraoperative prostate imaging. Med Phys. 2001;28:2551–2560. doi: 10.1118/1.1414009.

46. SHIRAZI-ADL SA, Shrivastava SC, Ahmed AM, Shirazi Adl SA, Shrivastava SC, Ahmed AM. Stress Analysis of the Lumbar Disc-Body Unit in Compression A Three-Dimensional Nonlinear Finite Element Study. Spine (Phila Pa 1976). 1984;9:120–134. doi: 10.1097/00007632-198403000-00003.
47. Dreischarf M, Zander T, Shirazi-Adl A, Puttlitz CM, Adam CJ, Chen CS, Goel VK, Kiapour A, Kim YH, Labus KM, et al. Comparison of eight published static finite element models of the intact lumbar spine: Predictive power of models improves when combined together. J Biomech. 2014;47:1757–1766. doi: 10.1016/j.jbiomech.2014.04.002. Cited: in: : PMID: 24767702.
48. SHIRAZI-ADL A, Ahmed AM, Shrivastava SC. Mechanical Response of a Lumbar Motion Segment in Axial Torque Alone and Combined with Compression. Spine (Phila Pa 1976). 1986;11:914–927. doi: 10.1097/00007632-198611000-00012.
49. Schmidt H, Kettler A, Heuer F, Simon U, Claes L, Wilke H-J. Intradiscal Pressure, Shear Strain, and Fiber Strain in the Intervertebral Disc Under Combined Loading. Spine (Phila Pa 1976). 2007;32:748–755. doi: 10.1097/01.brs.0000259059.90430.c2.
50. Lu YM, Hutton WC, Gharpuray VM. Do Bending, Twisting, and Diurnal Fluid Changes in the Disc Affect the Propensity to Prolapse? A Viscoelastic Finite Element Model. Spine (Phila Pa 1976). 1996;21.
51. Finley SM, Brodke DS, Spina NT, DeDen CA, Ellis BJ. FEBio finite element models of the human lumbar spine. Comput Methods Biomech Biomed Engin. 2018;21:444–452. doi: 10.1080/10255842.2018.1478967. Cited: in: : PMID: 30010415.
52. Shirazi Adl SA, Shrivastava SC, Ahmed AM. Stress Analysis of the Lumbar Disc-Body Unit in Compression A Three-Dimensional Nonlinear Finite Element Study. Spine (Phila Pa 1976). 1984;9:120–134. doi: 10.1097/00007632-198403000-00003.
53. Polikeit A, Nolte LP, Ferguson SJ. The Effect of Cement Augmentation on the

Load Transfer in an Osteoporotic Functional Spinal Unit. Spine (Phila Pa 1976). 2003;28:991–996. doi: 10.1097/01.BRS.0000061987.71624.17.

54. Zhang L, Yang G, Wu L, Yu B. The biomechanical effects of osteoporosis vertebral augmentation with cancellous bone granules or bone cement on treated and adjacent non-treated vertebral bodies: A finite element evaluation. Clin Biomech. 2010;25:166–172. doi: 10.1016/j.clinbiomech.2009.10.006. Cited: in: : PMID: 19917516.

55. Salvatore G, Berton A, Giambini H, Ciuffreda M, Florio P, Longo UG, Denaro V, Thoreson A, An KN. Biomechanical effects of metastasis in the osteoporotic lumbar spine: A Finite Element Analysis. BMC Musculoskelet Disord. 2018;19:38. doi: 10.1186/s12891-018-1953-6. Cited: in: : PMID: 29402261.

56. Shirazi-Adl A, Ahmed AM, Shrivastava SC. Mechanical Response of a Lumbar Motion Segment in Axial Torque Alone and Combined with Compression. Spine (Phila Pa 1976). 1986;11:914–927. doi: 10.1097/00007632-198611000-00012.

57. Silva MJ, Keaveny TM, Hayes WC. Load Sharing Between the Shell and Centrum in the Lumbar Vertebral Body. Spine (Phila Pa 1976). 1997;22.

58. Rohlmann A, Zander T, Rao M, Bergmann G. Applying a follower load delivers realistic results for simulating standing. J Biomech. 2009;42:1520–1526. doi: 10.1016/j.jbiomech.2009.03.048. Cited: in: : PMID: 19433325.

59. Rohlmann A, Bauer L, Zander T, Bergmann G, Wilke HJ. Determination of trunk muscle forces for flexion and extension by using a validated finite element model of the lumbar spine and measured in vivo data. J Biomech. 2006;39:981–989. doi: 10.1016/j.jbiomech.2005.02.019. Cited: in: : PMID: 16549091.

60. Akamaru T, Kawahara N, Sakamoto J, Yoshida A, Murakami H, Hato T, Awamori S, Oda J, Tomita K. The Transmission of Stress to Grafted Bone Inside a Titanium Mesh Cage Used in Anterior Column Reconstruction After Total Spondylectomy: A Finite-Element Analysis. Spine (Phila Pa 1976). 2005;30:2783–2787. doi: 10.1097/01.brs.0000192281.53603.3f.

61. Zhang Z, Fogel GR, Liao Z, Sun Y, Liu W. Biomechanical Analysis of Lateral Lumbar Interbody Fusion Constructs with Various Fixation Options: Based on a Validated Finite Element Model. World Neurosurg. 2018;114:e1120–e1129. doi: 10.1016/j.wneu.2018.03.158. Cited: in: : PMID: 29609081.

62. Zhou QK, Zeng FH, Tu JL, Dong ZQ, Ding ZH. Influence of cement-augmented pedicle screw instrumentation in an osteoporotic lumbosacral spine over the adjacent segments: A 3D finite element study. J Orthop Surg Res. 2020;15:132. doi: 10.1186/s13018-020-01650-5. Cited: in: : PMID: 32264901.
63. Guo H-Z, Guo D-Q, Tang Y-C, Liang D, Zhang S-C. Selective cement augmentation of cranial and caudal pedicle screws provides comparable stability to augmentation on all segments in the osteoporotic spine: a finite element analysis. Ann Transl Med. 2020;8:1384–1384. doi: 10.21037/atm-20-2246.
64. Allain J, Dufour T. Anterior lumbar fusion techniques: ALIF, OLIF, DLIF, LLIF, IXLIF. Orthop. Traumatol. Surg. Res. Elsevier Masson SAS; 2020. p. S149–S157.
65. Li JXJ, Phan K, Mobbs R. Oblique Lumbar Interbody Fusion: Technical Aspects, Operative Outcomes, and Complications. World Neurosurg. 2017;98:113–123. doi: 10.1016/j.wneu.2016.10.074. Cited: in: : PMID: 27777161.
66. Ambati D V., Wright EK, Lehman RA, Kang DG, Wagner SC, Dmitriev AE. Bilateral pedicle screw fixation provides superior biomechanical stability in transforaminal lumbar interbody fusion: A finite element study. Spine J. 2015;15:1812–1822. doi: 10.1016/j.spinee.2014.06.015. Cited: in: : PMID: 24983669.
67. Burkhart TA, Andrews DM, Dunning CE. Finite element modeling mesh quality, energy balance and validation methods: A review with recommendations associated with the modeling of bone tissue. J. Biomech. Elsevier; 2013. p. 1477–1488.
68. Zhu R, Niu W xin, Zeng Z li, Tong J hua, Zhen Z wei, Zhou S, Yu Y, Cheng L ming. The effects of muscle weakness on degenerative spondylolisthesis: A finite element study. Clin Biomech. 2017;41:34–38. doi: 10.1016/j.clinbiomech.2016.11.007. Cited: in: : PMID: 27918892.
69. Ilharreborde B, Shaw MN, Berglund LJ, Zhao KD, Gay RE, An KN. Biomechanical evaluation of posterior lumbar dynamic stabilization: An in vitro comparison between Universal Clamp and Wallis systems. Eur Spine J. 2011;20:289–296. doi: 10.1007/s00586-010-1641-1. Cited: in: : PMID: 21132335.
70. Rohlmann A, Neller S, Claes L, Bergmann G, Wilke HJ. Influence of a follower load on intradiscal pressure and intersegmental rotation of the lumbar spine. Spine

(Phila Pa 1976). 2001;26:E557-561. doi: 10.1097/00007632-200112150-00014.

71. Liang Z, Cui J, Zhang J, He J, Tang J, Ren H, Ye L, Liang D, Jiang X. Biomechanical evaluation of strategies for adjacent segment disease after lateral lumbar interbody fusion: Is the extension of pedicle screws necessary? BMC Musculoskelet Disord. 2020;21:117. doi: 10.1186/s12891-020-3103-1. Cited: in: : PMID: 32085708.
72. Zhong ZC, Hung C, Lin HM, Wang YH, Huang CH, Chen CS. The influence of different magnitudes and methods of applying preload on fusion and disc replacement constructs in the lumbar spine: A finite element analysis. Comput Methods Biomech Biomed Engin. 2013;16:943–953. doi: 10.1080/10255842.2011.645226. Cited: in: : PMID: 22224913.
73. Zhang Z, Li H, Fogel GR, Xiang D, Liao Z, Liu W. Finite element model predicts the biomechanical performance of transforaminal lumbar interbody fusion with various porous additive manufactured cages. Comput Biol Med. 2018;95:167–174. doi: 10.1016/j.compbiomed.2018.02.016. Cited: in: : PMID: 29501735.
74. Rohlmann A, Nabil Boustani H, Bergmann G, Zander T. Effect of a pedicle-screw-based motion preservation system on lumbar spine biomechanics: A probabilistic finite element study with subsequent sensitivity analysis. J Biomech. 2010;43:2963–2969. doi: 10.1016/j.jbiomech.2010.07.018: PMID: 20696430.
75. Sengul E, Ozmen R, Yaman ME, Demir T. Influence of posterior pedicle screw fixation at L4–L5 level on biomechanics of the lumbar spine with and without fusion: a finite element method. Biomed Eng Online. 2021;20:98. doi: 10.1186/s12938-021-00940-1. Cited: in: : PMID: 34620170.
76. Chen LH, Tai CL, Lee DM, Lai PL, Lee YC, Niu CC, Chen WJ. Pullout strength of pedicle screws with cement augmentation in severe osteoporosis: A comparative study between cannulated screws with cement injection and solid screws with cement pre-filling. BMC Musculoskelet Disord. 2011;12:1–11. doi: 10.1186/1471-2474-12-33. Cited: in: : PMID: 21284883.
77. Wang W, Baran GR, Garg H, Betz RR, Moumene M, Cahill PJ. The benefits of cement augmentation of pedicle screw fixation are increased in Osteoporotic bone: A finite element analysis. Spine Deform. 2014;2:248–259. doi: 10.1016/j.jspd.2014.03.002.

78. Wang B, Hua W, Ke W, Lu S, Li X, Zeng X, Yang C. Biomechanical evaluation of transforaminal lumbar interbody fusion and oblique lumbar interbody fusion on the adjacent segment: a finite element analysis. World Neurosurg. 2019;126:e819–e824. doi: 10.1016/j.wneu.2019.02.164. Cited: in: : PMID: 30862579.
79. Song C, Chang H, Zhang D, Zhang Y, Shi M, Meng X. Biomechanical Evaluation of Oblique Lumbar Interbody Fusion with Various Fixation Options: A Finite Element Analysis. Orthop Surg. 2021;13:517–529. doi: 10.1111/os.12877.
80. Yao J, Burns JE, Forsberg D, Seitel A, Rasoulian A, Abolmaesumi P, Hammernik K, Urschler M, Ibragimov B, Korez R, et al. A multi-center milestone study of clinical vertebral CT segmentation. Comput Med Imaging Graph. 2016;49:16–28. doi: 10.1016/j.compmedimag.2015.12.006. Cited: in: : PMID: 26878138.
81. Michael Smith. ABAQUS/Standard User's Manual, Version 6.9. United States: "Dassault Syst{\`e}mes Simulia Corp";
82. Quillo-Olvera J, Lin G-X, Jo H-J, Kim J-S. Complications on minimally invasive oblique lumbar interbody fusion at L2–L5 levels: a review of the literature and surgical strategies. Ann Transl Med. 2018;6:101–101. doi: 10.21037/atm.2018.01.22.
83. McDonald K, Little J, Pearcy M, Adam C. Development of a multi-scale finite element model of the osteoporotic lumbar vertebral body for the investigation of apparent level vertebra mechanics and micro-level trabecular mechanics. Med Eng Phys. 2010;32:653–661. doi: 10.1016/j.medengphy.2010.04.006. Cited: in: : PMID: 20439162.
84. Margulies JY, Payzer A, Nyska M, Neuwirth MG, Floman Y, Robin GC. The Relationship Between Degenerative Changes and Osteoporosis in the Lumbar Spine. Clin Orthop Relat Res. 1996;324.
85. Palepu V, Helgeson MD, Molyneaux-Francis M, Nagaraja S. The effects of bone microstructure on subsidence risk for ALIF, LLIF, PLIF, and TLIF spine cages. J Biomech Eng. 2019;141. doi: 10.1115/1.4042181. Cited: in: : PMID: 30516247.
86. Parisien A, Wai EK, Elsayed MSA, Frei H. Subsidence of Spinal Fusion Cages: A Systematic Review. Int J Spine Surg. 2022;16:1103–1118. doi: 10.14444/8363.
87. Hu Z, He D, Gao J, Zeng Z, Jiang C, Ni W, Yik JHN, Zhao X, Fan S. The Influence of Endplate Morphology on Cage Subsidence in Patients With Stand-Alone

Oblique Lateral Lumbar Interbody Fusion (OLIF). Glob Spine J. 2023;13:97–103. doi: 10.1177/2192568221992098.

88. Marchi L, Abdala N, Oliveira L, Amaral R, Coutinho E, Pimenta L. Radiographic and clinical evaluation of cage subsidence after stand-alone lateral interbody fusion. J Neurosurg Spine. 2013;19:110–118. doi: 10.3171/2013.4.SPINE12319. Cited: in: : PMID: 23662890.

89. Le T V., Baaj AA, Dakwar E, Burkett CJ, Murray G, Smith DA, Uribe JS. Subsidence of Polyetheretherketone Intervertebral Cages in Minimally Invasive Lateral Retroperitoneal Transpsoas Lumbar Interbody Fusion. Spine (Phila Pa 1976). 2012;37:1268–1273. doi: 10.1097/BRS.0b013e3182458b2f.

90. Rastegar S, Arnoux PJ, Wang X, Aubin CÉ. Biomechanical analysis of segmental lumbar lordosis and risk of cage subsidence with different cage heights and alternative placements in transforaminal lumbar interbody fusion. Comput Methods Biomech Biomed Engin. 2020;23:456–466. doi: 10.1080/10255842.2020.1737027. Cited: in: : PMID: 32169009.

91. Calvo-Echenique A, Cegoñino J, Chueca R, Pérez-del Palomar A. Stand-alone lumbar cage subsidence: A biomechanical sensitivity study of cage design and placement. Comput Methods Programs Biomed. 2018;162:211–219. doi: 10.1016/j.cmpb.2018.05.022. Cited: in: : PMID: 29903488.

92. Han Z, Ma C, Li B, Ren B, Liu J, Huang Y, Qiao L, Mao K. Biomechanical studies of different numbers and positions of cage implantation on minimally invasive transforaminal interbody fusion: A finite element analysis. Front Surg. 2022;9:1011808. doi: 10.3389/fsurg.2022.1011808.

93. Klibanski A, Adams-Campbell L, Bassford T, Blair SN, Boden SD, Dickersin K, Gifford DR, Glasse L, Goldring SR, Hruska K, et al. Osteoporosis prevention, diagnosis, and therapy. J Am Med Assoc. American Medical Association; 2001. p. 785–795. Available from: https://pure.johnshopkins.edu/en/publications/osteoporosis-prevention-diagnosis-and-therapy-4.

94. Ponnusamy KE, Iyer S, Gupta G, Khanna AJ. Instrumentation of the osteoporotic spine: Biomechanical and clinical considerations. Spine J. Elsevier; 2011. p. 54–63.

95. Charnley J. A Biomechanical Analysis of the use of cement to anchor the femoral head Prosthesis. J Bone Joint Surg Br. 1965;47:354–363. doi: 10.1302/0301-620x.47b2.354. Cited: in: : PMID: 14302740.
96. Elder BD, Lo SFL, Holmes C, Goodwin CR, Kosztowski TA, Lina IA, Locke JE, Witham TF. The biomechanics of pedicle screw augmentation with cement. Spine J. Elsevier Inc.; 2015. p. 1432–1445.
97. Park J, Ham DW, Kwon BT, Park SM, Kim HJ, Yeom JS. Minimally Invasive Spine Surgery: Techniques, Technologies, and Indications. Asian Spine J. 2020;14:694–701. doi: 10.31616/asj.2020.0384.
98. Goldstein CL, Macwan K, Sundararajan K, Rampersaud YR. Perioperative outcomes and adverse events of minimally invasive versus open posterior lumbar fusion: Meta-analysis and systematic review. J. Neurosurg. Spine. American Association of Neurological Surgeons; 2016. p. 416–427. Available from: http://thejns.org/doi/abs/10.3171/2015.2.SPINE14973.
99. Wang X, Borgman B, Vertuani S, Nilsson J. A systematic literature review of time to return to work and narcotic use after lumbar spinal fusion using minimal invasive and open surgery techniques. BMC Health Serv Res. 2017;17:446. doi: 10.1186/s12913-017-2398-6. Cited: in: : PMID: 28655308.
100. Zhang J, Wang G, Zhang N. A meta-analysis of complications associated with the use of cement-augmented pedicle screws in osteoporosis of spine. Orthop. Traumatol. Surg. Res. Elsevier Masson s.r.l.; 2021. p. 102791.
101. Zeng T-H, Wang Y-M, Yang X-J, Xiong J-Y, Guo D-Q. The clinical comparative study on high and low viscosity bone cement application in vertebroplasty. Int J Clin Exp Med. 2015;8:18855–18860. Cited: in: : PMID: 26770507.
102. Tang S, Fu W, Zhang H, Zhang H, Liang B. Efficacy and Safety of High-Viscosity Bone Cement Vertebroplasty in Treatment of Osteoporotic Vertebral Compression Fractures with Intravertebral Cleft. World Neurosurg. 2019;132:e739–e745. doi: 10.1016/j.wneu.2019.08.029. Cited: in: : PMID: 31415893.
103. Zhu SY, Zhong ZM, Wu Q, Chen JT. Risk factors for bone cement leakage in percutaneous vertebroplasty: a retrospective study of four hundred and eighty five patients. Int Orthop. 2016;40:1205–1210. doi: 10.1007/s00264-015-3102-2. Cited: in: : PMID: 26753843.

9. BIBLIOGRAPHY OF THE CANDIDATE'S PUBLICATIONS

Publications that formed the basis of the dissertation:

1. **Bereczki F**, Turbucz M, Kiss R, Eltes PE, Lazary A. Stability Evaluation of Different Oblique Lumbar Interbody Fusion Constructs in Normal and Osteoporotic Condition – A Finite Element Based Study. Front Bioeng Biotechnol 2021;9:1013. https://doi.org/10.3389/fbioe.2021.749914.
2. **Bereczki F**, Turbucz M, Pokorni AJ, Hajnal B, Rónai M, Klemencsics I, et al. The effect of polymethylmethacrylate augmentation on the primary stability of stand-alone implant construct versus posterior stabilization in oblique lumbar interbody fusion with osteoporotic bone quality– a finite element study. Spine J 2024;0. https://doi.org/10.1016/j.spinee.2024.01.021.

Publications in the field of In Silico Medicine/Musculoskeletal modelling as co-author:

1. Fayad J, Turbucz M, Hajnal B, **Bereczki F**, Bartos M, Bank A, et al. Complicated Postoperative Flat Back Deformity Correction With the Aid of Virtual and 3D Printed Anatomical Models: Case Report. Front Surg 2021;8:662919. https://doi.org/10.3389/fsurg.2021.662919.
2. Eltes PE, Kiss L, Bartos M, Gyorgy ZM, Csakany T, **Bereczki F**, et al. Geometrical accuracy evaluation of an affordable 3D printing technology for spine physical models. J Clin Neurosci 2020;72:438–46. https://doi.org/10.1016/j.jocn.2019.12.027.
3. Techens C, **Bereczki F**, Montanari S, Lazary A, Cristofolini L, Eltes PE. Assessment of foraminal decompression following discoplasty using a combination of ex vivo testing and numerical tools. Sci Rep 2023;13:1–10. https://doi.org/10.1038/s41598-023-27552-0.
4. Eltes PE, Turbucz M, Fayad J, **Bereczki F**, Szőke G, Terebessy T, et al. A Novel Three-Dimensional Computational Method to Assess Rod Contour Deformation and to Map Bony Fusion in a Lumbopelvic Reconstruction After En-Bloc Sacrectomy. Front Surg 2022;8:698179. https://doi.org/10.3389/fsurg.2021.698179.

5. Techens C, Montanari S, **Bereczki F**, Eltes PE, Lazary A, Cristofolini L. Biomechanical consequences of cement discoplasty: An in vitro study on thoraco-lumbar human spines. Front Bioeng Biotechnol 2022;10:1040695. https://doi.org/10.3389/fbioe.2022.1040695.
6. Hajnal B, Eltes PE, **Bereczki F**, Turbucz M, Fayad J, Pokorni AJ, et al. New method to apply the lumbar lordosis of standing radiographs to supine CT-based virtual 3D lumbar spine models. Sci Rep 2022;12:20382. https://doi.org/10.1038/s41598-022-24570-2.
7. Eltes PE, Kiss L, **Bereczki F**, Szoverfi Z, Techens C, Jakab G, et al. A novel three-dimensional volumetric method to measure indirect decompression after percutaneous cement discoplasty. J Orthop Transl 2021;28:131–9. https://doi.org/10.1016/j.jot.2021.02.003.

Publications in the field of Spine Surgery/Genetics as co-author:

1. Kiss L, Szoverfi Z, **Bereczki F**, Eltes PE, Szollosi B, Szita J, et al. Impact of Patient-specific Factors and Spinopelvic Alignment on the Development of Adjacent Segment Degeneration After Short-segment Lumbar Fusion. Clin Spine Surg A Spine Publ 2023;36:E306–10. https://doi.org/10.1097/BSD.0000000000001369.
2. Biczo A, **Bereczki F**, Koch K, Varga PP, Urban J, Fairbank J, et al. Genetic variants of interleukin 1B and 6 are associated with clinical outcome of surgically treated lumbar degenerative disc disease. BMC Musculoskelet Disord 2022;23:1–11. https://doi.org/10.1186/s12891-022-05711-0.

10. ACKNOWLEDGEMENTS

I would like to express my deepest gratitude to my Supervisors: Péter Endre Éltes, M.D. PhD the head of the In Silico Biomechanical Laboratory for his dedication and unwavering support in guiding me through the perilous process of in silico, Finite Element modeling. No matter the time, weekends, or holidays he always found time to answer my questions and discuss topics, potential research ideas. I thank Áron Lazáry M.D. PhD for providing invaluable guidance throughout my doctoral journey and granting insight into the aspects of clinical research. Your expertise, constructive feedback, and dedication have been instrumental in shaping the direction of this research and enhancing its quality.

Thank you kindly for granting me the privilege to study and work within the invigorating and dedicated setting of the ISBL, R&D department at the National Center for Spinal Disorders.

I would like to thank Péter Pál Varga, MD, Zoltan Hoffer M.D., and my Supervisors for creating the infrastructure required for in silico modelling within The National Center for Spinal Disorders.

I express my gratitude to the members of In Silico Biomechanics Laboratory for their constant support, inspiring discussions, and pleasant working atmosphere. Mate Turbucz, Benjamin Hajnal, Ágoston Pokorni, Jannifer Fajad, Chloé Techens.

I am grateful to my fellow colleagues working in the R&D department and friends who have provided a supportive network during this challenging undertaking. Thank you for your encouragement, intellectual discussions, and sharing of experiences, which have significantly enriched my research and personal growth.

I am indebted to the staff and spine surgeons of The National Center for Spinal Disorders, whose contributions and support have been invaluable throughout my academic journey. Their encouragement, resources, and administrative assistance have played a crucial role in fostering an enriching research environment.

Lastly, I want to express my heartfelt appreciation to my family and loved ones for their unwavering support, love, and understanding. Your encouragement and belief in me have been the driving force behind this accomplishment. Your constant presence, patience, and understanding during my moments of stress and uncertainty have been truly remarkable.